may have occurred during earlier Quaternary time (Seismotectonic Framework report [USGS, written communication, 1996]). Measurements of net slip displacements vary widely among individual events and from one study site to another, with values ranging from 28 to 167 cm for a single Quaternary event. Cumulative Quaternary displacement ranges from 1.7 to 7.8 m locally. Age determinations for the various events differ from one site to another, with the most recent event ranging from 5 to 90 ka and the next youngest ranging from 70 to 150 ka. Values of recurrence intervals based on the combined age data for all three study sites range from 21 to 118 ky. Our preferred slip rate for the entire fault is 0.008 m/kyr. The slip rate is a mid-Pleistocene rate inferred from the exposures at Busted butte. Menges (Seismotectonic Framework report [USGS, written communication, 1996]) estimates the offset at the base of the strata there as 5.22 m to 7.62m; an approximate mean value of 6.4 m is used for the preferred value. The age of the base of these sediments is interpreted to be about 740 ka, based on exposure of the Bishop ash.

**Stagecoach Road Fault**

The minimum fault length, as mapped by Simonds *et al.* (1995) from Stagecoach Road south, is 4.5 km. However, if we extend it north to join the Paintbrush Canyon fault near the south end of Busted Butte, and extend it south to the dissected escarpment near Wells Cone, the maximum inferred length is 11 km. We take it to the most southerly mapped fault scarp for a preferred distance of 9 km. The minimum segment is expressed as discontinuous scarps in mid-Pleistocene alluvium; the south end of this trace is concealed by undeformed Holocene sediment. Alluvium of late Quaternary age is displaced 1.0 to 2.3 m; slickensides indicate chiefly dip slip. Bedrock displacement is estimated to be 400 to 600 m down-to-the-west (Scott, 1990). Average dip is 73 degrees west. Trench excavations display evidence for three to seven episodes of Quaternary faulting (Seismotectonic Framework report [USGS, written communication, 1996]). The two youngest events have been dated at 5 to 15 ka and 20 to 30 ka, respectively. Two earlier events may have occurred in late Pleistocene time, the oldest about 110 ka. The age relationships indicate preferred values of recurrence intervals in the range of 10 to 35 ky, and slip rates of 0.0057 to 0.028 m/kyr. The slip rates are calculated from data reported in the Seismotectonic Framework report (USGS, written communication, 1996) for trench SCR-T3. Here, our inferred range of dip-slip offset is 0.67 m to 2.7 m, corrected for hanging wall rollover. The offset unit, G2, has a U-series date of 108±10 ka.

**Solitario Canyon Fault**

The Solitario Canyon fault is a block-bounding fault that defines the west side of the potential repository block. Displacement along most of the fault trace is down-to-the-west, with offsets of more than 500 m. Average dip of the fault plane is 72 degrees west. At the north end, the fault dips east, and displacement is 61 m down-to-the-east (Scott and Bonk, 1984). From a north terminus on the south flank of Yucca Wash on south to the hingeline, it is a well-defined fault zone 14.8 km long. Farther south, it loses topographic definition and splays into three or more faults that distribute the total displacement (W. C. Day, USGS, written communication, 1997). South of the hingeline, the main fault trace may regather and strike west of south to join up with the Windy Wash fault (W. C. Day *et al.*, unpub. map); or it may trend east of south and merge with the Stagecoach Road fault. On the basis of aeromagnetic data, we infer that it becomes a buried fault--possibly a graben-bounding fault--that continues south, parallel to the Stagecoach Road fault, for a maximum length of 21.5 km. Our preferred length is 18.5 km for Stagecoach Road fault linkage option, based on mapping by Simonds *et al.* (1995). The fault appears to become more shallow in dip and more zonal in general as it extends south from the elevated area of the Prow, exposing more footwall on strike. Opposite the potential repository block, the footwall includes an attenuated slice 3.5 km long and about 200 m wide broken by complex scarps and local faults. The slice is sampled by trenches T4 and T5. The character of the main fault trace is unclear along this segment. Eleven trenches and one natural wash exposure have been excavated across or near the Solitario Canyon fault, exposing evidence that suggests as many as four paleoseismic events dated at 20 to 30, 70 to 80, 120 to 250, and 150 to 250 ka, respectively, took place along the fault (Seismotectonic Framework report [USGS, written communication, 1996]). There is also indication that two episodes of fracturing postdate the most recent event; these fracturing episodes are interpreted as being associated with moderate-sized earthquakes on the Solitario Canyon fault or with earthquakes on nearby or regional faults. Characteristics of the affected surficial deposits suggest that the fractures developed in Holocene and/or latest Pleistocene time. A recurrence interval of 35 ky is considered a minimum (two events within the past 70 to 80 ka and four within the past 150 ka). Estimates of cumulative displacement over 150 to 250 ky range from 1.8 m (from scarp measurements and trench logs) to 2.6 m (from trench logs). Our preferred average slip rate for the fault is 0.015 m/kyr, based on a preferred soil correlation age of 200 ka.

**Iron Ridge Fault**

The Iron Ridge fault is what Day *et al.* (written commun.) term a relay fault. Its minimum (and preferred) length of 8.3 km spans the distance between its juncture with the Solitario and Stagecoach Road faults. However, the Iron Ridge fault is well defined only along the western edge of Iron Ridge. The north and south termini are frayed out for a kilometer or more along strike; and it is possible that, at the south end, the main trace projects south to merge with the (buried) Solitario Canyon fault. If so, this gives a maximum length of 10 km. However, Iron Ridge is terminated at the hingeline, where the fault jogs east for a kilometer, around the nose of the truncated ridge, bringing the ridge-bounding fault trace within 500 m of the Stagecoach Road fault. For half its length, the Iron Ridge fault forms a bedrock-alluvial contact with prominent scarps. Displacement is chiefly dip-slip, down to the west on a fault plane that dips 70 degrees. At least one locality shows multiple late-Quaternary faulting (Simonds *et al.*, 1995). The Iron Ridge fault is a complex and damaged zone of normal faults that have numerous splays and flare-off fractures (including the Abandoned Wash fault). As such, it simply may be the most prominent of a wide zone of linked-bridging faults that have formed in response to extension and left-lateral shear between the Solitario and Stagecoach Road faults. Its seismogenic significance is questionable; it may be confined to the carapace (minimum width of about 2 km) or at least not extend deeply into the Paleozoic substrate as a single-plane (about 5 km). A.R. Ramelli (written communication, 1996) estimates 2 m of offset has occurred since mid-Quaternary, but considering erosion over this time, the offset could range from 1.7 m to 2.2 m. Ramelli correlates the offset unit with deposits that make up the Solitario surface of Peterson *et al.* (1995). This surface ranges in age from 433 ka to 730 ka. To calculate our preferred slip rate (0.0033m/kyr) we chose a mid-point age of 600 ka. Smaller displacements (0.5, 0.7, 1 m; Table SDO-5) are reported from trench SCF-T2 observations (Seismotectonic Framework report [USGS, written communication, 1966]).

**Fatigue Wash Fault**

The Fatigue Wash fault is a north- to northeast-striking, down-to-the-west normal to steep oblique fault located about 3.5 km west of the potential repository. From its south merger with the Windy Wash fault to a possible northern merger with the Windy Wash fault at the south end of West Ridge, it has a minimum length of 12 km. It also could be carried north along a deep notch that defines the east side of West Ridge to the Prow, where it frays out in a plexus of normal faults and graben. The longest trace through this area takes it into the

caldera rim zone, for a maximum length of 22 km. We prefer 18 km because of uncertainty in the north termination. The Fatigue Wash fault is remarkably parallel to the Windy Wash fault, which lies only about a kilometer to the west, along the west flank of West Ridge. It probably is not a major fault despite its considerable length. Its geometry and association with bridge faults to the Windy Wash fault suggests that the Fatigue Wash fault is either: (1) one or more linked slices of the footwall of the Windy Wash fault, formed in response to Windy Wash faulting, or (2) a parallel subsidiary fault that merges with the Windy Wash fault beneath the carapace. The fact that Fatigue Wash fault merges with the south Windy Wash fault strongly implies that the Northern and Southern Windy Wash faults are indeed a single continuous fault, or at least linked faults, the middle (linking) part of which is buried but which apparently forms a graben in association with the Fatigue Wash fault in the vicinity of the hingeline. Average dip of the fault plane is 73 degrees, and displacement is about 72 m (Scott and Bonk, 1984). Three to six paleoseismic events (five being the preferred number) are documented by the stratigraphic and structural relations exposed in two trenches excavated in Quaternary deposits along the fault trace. Four of the preferred events occurred after 730 ka. The two most recent events probably took place between 20 to 70 ka, suggesting a late-Quaternary clustering of earthquakes. An estimate of the long-term average recurrence interval ranges from 120 to 250 ky, with a preferred value of 185 ky. Two meters of cumulative vertical displacement during the last four events indicate a Quaternary slip rate of 0.002 ± 0.0001 m/kyr. Data from measurements on scarps outside the trenches indicate a greater Quaternary slip rate of 0.009 ± 0.006 m/kyr (Seismotectonic Framework report, [USGS, written communication, 1996]). Offsets at trench SP5 were measured by projection of intact correlative surfaces to give values of 2.8 and 3.9 m of nomal displacement. A minimum value of 2.5 m of vertical separation is estimated based on uncertainties of scarp measurement and surface projection. The fault scarp is developed in the Solitario surface of Peterson *et al.* (1995) which is estimated to have and age range of 433 ka to 739 ka, with a preferred age of 600 ka.

**Windy Wash Fault**

We consider the north-striking Windy Wash fault to be a segmented or linked block-bounding fault. The north strand extends from the Prow south for 9 km. It can be carried north of the Prow into the caldera rim zone an additional 2 km, but we prefer a length of 9 km to accommodate the uncertainties. The south strand extends south from trench CF2 for

8 km as a well-defined fault trace (Simonds *et al.*, 1995). It can be carried farther south by linking scarp segments for a preferred length of 11.5 km. If we carry it north of trench CF2 (along an east-facing scarp; Simonds *et al.*, 1995), we obtain a maximum length of 12.5 km. The total maximum length of the linked north and south segments is about 24 km. Apart from the central, down-to-the-east scarp in alluvium, the fault has down-to-the-west displacement of a few hundred meters (Scott, 1990). Average dip of the fault is 63 degrees to the west, and offset is chiefly dip slip; but locally both right and left oblique slip have occurred. Evidence of Quaternary displacement is limited to subtle scarps in alluvium and to fractures in hanging walls of fault line scarps. Three trenches were excavated across scarps in alluvium along the central part of the fault (USGS, written communication, 1996). One trench displays evidence of eight coseismic surface ruptures during Quaternary time; the other two display evidence of five ruptures. Mid- to late-Pleistocene gravel in one trench is displaced about a meter down-to-the-west, and Holocene silt above the main fault plane is ruptured. Dating of soils and fine silt deposits indicates that the surface faulting along the Windy Wash fault took place about 3, 40, 75, 150, 200, 240, 340, and 400 ka (preferred values or mid-points of the ranges of event timing). The recurrence interval of faulting for the last four events is about 40 to 50 ky, and between 50 to 57 ky for the longer record; the preferred recurrence interval is 40 ky. Total net displacement on the oldest hanging wall deposit is 3.67 m with an uncertainty of ± 0.3 m. U-series ages constrain the offset unit to be at least 300 ka old, and as much as 400 ka (USGS, written communication, 1996), indicating a long-term average slip rate ranging from 0.009 to 0.017 m/kyr. Displacements measured in trench CF-2 are 0.6 m to a maximum value of 0.88 m (USGS, written communication, 1996). A 1 m offset is proposed on the basis that the trench may not be sited at a point of maximum displacement.

In addition to the faults described above, several other faults at the site may penetrate the carapace, but in our evaluation these are capable of generating maximum earthquakes only at or below MBE levels of moment magnitude 6.4 ± 0.2; thus, these faults are considered to be covered by the background seismicity. Several of these faults are used in the linked and distributed event scenarios developed for this analysis. These include the Bow Ridge, Ghost Dance, Abandoned Wash, Northern Crater Flat, and Southern Crater Flat faults. Although these faults are considered not capable of individually generating an earthquake larger than

the maximum background, by virtue of linkage or distributed connections they may make a small contribution to some of the earthquake scenario parameters.

**Bow Ridge Fault**

The Bow Ridge fault has been called a block-bounding fault (W. C. Day, written communication, 1998), but little is known about it except that it is a largely alluvium-covered, north-striking, west-dipping normal fault that lies along the east side of the potential repository block for a length of 7 km. It is exposed only along the west side of Bow Ridge and Exile Hill (site of trench 14) and in the ESF. Structure at Bow Ridge is complex, marked by breccia and small graben; a throughgoing fault that defines the arcuate scarp face of Bow Ridge is strongly suggested. Its shape and bounding structure imply that the Bow Ridge fault, as an inferred single-plane fault, arcs abruptly east to merge with the Paintbrush Canyon fault. However, the Bow Ridge fault may simply represent an assemblage of variously striking fault segments, all part of hanging wall damage associated with the Paintbrush fault. The fault is defined in places along the west side of Exile Hill by a fault line scarp and a bedrock-colluvium contact (Simonds *et al.*, 1995). Here, Tertiary volcanic rocks show about 125 m of down-to-the-west displacement along a 65- to 75-degree, west-dipping, left-oblique fault plane. North of Isolation Ridge, the Bow Ridge fault has east-side-down displacement. A series of trenches has been excavated to reveal a complex fault zone developed in highly fractured Tertiary volcanic rock and Quaternary colluvial deposits. Several faulting events are evident in the surficial units, the oldest more than 700 ka and two younger events 130 to 150 ka and 30 to 130 ka, respectively. A minimum age of 48 ± 20 ka is established for the youngest displacement. Cumulative dip-slip displacement of the Quaternary deposits ranges from 30 to 45 cm (considering an oblique slip component, net slip is 33 to 70 cm). Preferred values for average recurrence intervals of faulting events range from 100 to 140 ky. Slip rates range from 0.002 to 0.007 m/kyr, with a preferred value of 0.003 m/kyr.

**Ghost Dance Fault**

The Ghost Dance fault strikes north through the central part of the repository block between Wren Wash on the north and Abandoned Wash on the south, a distance of 3.7 km. The fault is not exposed as a single-plane feature, but consists of three right-stepping segments. The north segment is 660 m long; it extends south to Split Wash, is 2 to 4 m wide, and has as

much as 6 m displacement down-to-the-west. The central segment is 450 m long; it extends from Live Yucca Ridge to Antler Ridge, forms a zone of breccia-filled splays from 1 to 2 m thick over a zone as much as 150 m wide, and has as much as 20 m down-to-the-west displacement. The south segment is 830 m long; it extends to Broken Limb Ridge, forms a breccia zone as much as 55 m wide, and has about 27 m of down-to-the-west displacement. Near Broken Limb Ridge, the fault bifurcates, the most prominent and continuous branch extending southwest for 1.5 km to apparently link with the Abandoned Wash fault of Scott and Bonk (1984) at Abandoned Wash. The Ghost Dance fault does not physically connect with the Abandoned Wash fault; it more or less comes into alignment with the local slip planes that comprise the north extent of the Abandoned Wash fault (W. C. Day, USGS, written communication, 1996).

The amount of brecciation and offset along the Ghost Dance fault decrease in the vicinity of the ESF and Ghost Dance Wash (a 2- to 15-m wide breccia zone; 3 to 6 m of offset); but displacement increases with proximity to the Abandoned Wash fault (as much as 17 m). Throughout its length, the Ghost Dance fault ranges in dip from vertical to 75 degrees west and is characterized by one or more breccia zones of variable thickness. The breccia typically is uncemented or an open fretwork that shows little or no evidence of size or shape segregation or milling due to shear. The Ghost Dance fault has no aeromagnetic signature and only small, low-amplitude gravity lows along the hanging wall (C. J. Potter *et al.*, written commun.).

Four trenches have been excavated in Quaternary sediment across projected traces of the Ghost Dance fault, but no offset of any of these deposits has been observed. In one trench, for example, 40 to 50 cm of unfaulted latest Pleistocene to early Holocene (age 82.8 ± 1.9 to 9.6 ±0.1 ka) slope-wash colluvium and fine-grained eolian deposits can be seen to overlie faulted and fractured tuff. A discontinuous fracture, however, was observed in a highly calcified horizon draped over bedrock in one trench; but it does not extend upward through the overlying units. Age relations suggest that the fracturing must have occurred at least 82 ka; the fracture may have resulted from a seismic event on any number of faults in the area. The non-integration of the fault segments along strike; the brecciated, zonal character and the poorly defined, fayed fault terminations; and the lack of shear tooling or shear segregation within and along the fault breaks, all indicate that the rock broke with minor

offset during a single, short-lived failure event and has not undergone subsequent deformation that might have modified the initial damage.

We interprete the Ghost Dance fault as a tear fault confined to the carapace. It is considered to have resulted from clockwise torque and bending applied to the central block during the initial to peak phase of vertical axis rotation. C. J. Potter *et al.* (written commun.) deduce that the right steps may be controlled by pre-existing sets of closely spaced, northwest-striking cooling joints. Because the Ghost Dance fault is a relic of ancient tensile failure and has virtually no cohesive strength, it is a locus of tensile strain for overlying cohesive strata and likely will remain so as long as extension dominates the stress regime at Yucca Mountain.

**Abandoned Wash Fault**

The Abandoned Wash fault is essentially a 6-km-long zone of small normal faults and horsts and graben of negligible offset that connects the Ghost Dance and the Solitario Canyon faults. It probably is structurally and genetically akin to the Ghost Dance fault and is confined to the carapace. Its presence is marked by deep erosion. Where it crosses ridge divides and especially at its junction with the Solitario Canyon fault, there is little geomorphic indication of offset.

**Northern Crater Flat Fault**

The Northern Crater Flat fault is a poorly defined structure that appears to consist of aligned horsts and graben in a zone about 600 m wide. Dominant displacement is down-to-the-west normal or normal oblique. It trends north to northeast along the east side of Crater Flat, about 5 km west of the potential repository. As mapped (Simonds *et al.*, 1995), the maximum length is about 12 km. It terminates to the south at the hingeline and frays out to the north among normal faults within the caldera rim zone. Its location implies that it is antithetic to Bare Mountain fault; hence, we infer a relatively small fault width. Only one of the two trenches excavated across the center of the projected trace of the fault intersected the fault. Stratigraphic and structural evidence for as many as five paleoearthquake events was observed in this trench. On the basis of a minimum age of 500 ka for the oldest exposed Quaternary unit and an estimate of less than 10 ka (preliminary age date of 5.46 ± 1.4 ka) for the most recent faulting event, a possible range in average recurrence interval is 120 to

160 ky. Cumulative displacement for all five events is about 160 cm, indicating a slip rate of 0.003 m/kyr since the earliest event.

**Southern Crater Flat Fault**

The Southern Crater Flat fault is a north- to northeast-striking, normal fault that is down to the west, and has a left-slip component. It is defined by a basalt-alluvium contact, fractured carbonate-cemented alluvium, subtle scarps in alluvium, and a linear stream channel (Simonds *et al.*, 1995). North of trench CFFT1, the fault trace is subtle. It projects toward convergence with the north end of the Southern Windy Wash fault. Alternatively, the north end of the Southern Crater Flat fault could be offset 1.5 km east of the Northern Crater Flat fault by slip along the hingeline. The Southern Crater Flat fault can be traced south for a maximum of about 15 km. The minimum length, as mapped by Simonds *et al.* (1995), is 6 km. The amount of offset is unknown; slickensides on a plane that dips 70 degrees indicate left-oblique movement. Two trenches were excavated across the Southern Crater Flat fault, exposing alluvial gravel deposits that contain accumulations of fine-grained aeolian material. There is evidence that at least three paleoseismic events occurred during the Quaternary, for a total measured offset of 24 to 65 cm. Preliminary age determinations of the alluvial materials and of opaline silica collected from the inner rinds of clasts indicate that the oldest event occurred 130 to 250 ka, the next 10 to 60 ka, and the youngest 2 to 6 ka. Minimum recurrence intervals are in the range of 5 to 60 ky; the estimated maximum vertical slip rate is 0.002 m/kyr.

### 3.4.1 Event Scenarios: Single Faults, Linked Faults, and Distributed Faults

For local faults, three types of maximum earthquake models, or scenarios, are considered: single fault, linked fault, and distributed fault scenarios. Single-fault scenarios are given for the six local (i.e., Yucca Mountain) faults identified for this analysis (Figure SDO-7a). Linked-fault scenarios were developed by considering direct structural linkages and indications of potential event correlation between adjacent faults (Figure SDO-7b). Earthquake lengths are based on the end-to-end length of the combined fault plane segments. Distributed-fault scenarios involve parallel faults that slip together. For distributed fault scenarios, maximum surface displacements are combined in a cross-strike fashion, and lengths may or may not be increased over single-fault scenarios. All event scenarios, individual fault, linked faults, and distributed faults, are presented in Appendix SDO-1. Six

faults are involved, and one (Paintbrush Canyon) has two earthquake segment alternatives. Thus, there can be seven individual fault scenarios. Nine combinations of faults are modeled for the linked scenarios (Figure SDO-7b), and eight combinations of faults are modeled for the distributed fault scenarios. The relative weighting of each scenario is expressed in the occurrence rates given in Appendix SDO-1; the generation of these occurrence rates is discussed in section 3.3.3 on earthquake recurrence.

### 3.4.2 Fault Source Parameters for Maximum Magnitude

Fault source parameters are the basic, quantitative components needed to estimate the maximum earthquake a mapped fault is capable of generating. We estimate maximum earthquake magnitudes on the basis of as many parameters as possible to mitigate the uncertainties inherent in any individual parameter. An attempt is made to capture the uncertainties of the input values by using minimum and maximum values along with preferred values; various observational uncertainties are considered to be accounted for in empirical relationships relating fault parameters to magnitude. We consider the fault parameters we measure at the surface to be representative of the seismogenic structure at depth. For each scaling parameter, either an empirical relationship or an equation is used to scale magnitude from the input parameters. For the final value, we averaged the results for our magnitude estimates.

Using multiple magnitude estimation techniques provides the epistemic uncertainty to the final value. To characterize some of the aleatory uncertainty that also exists, each final value is considered to have an uncertainty of $\pm$ 0.25 magnitude units. This is a comparable value to the standard deviations of the regressions used to scale earthquake magnitude.

A logic tree (Figure SDO-8) was designed on the simplest sequence of parameter decisions necessary and justified by the data. The sizes of potential maximum earthquakes were scaled using fault length, fault width, maximum surface displacement, length times maximum surface displacement, fault area, length and slip rate, and calculations of seismic moment. Measured values are ordered in our assessments (Table SDO-4) and weighted on the basis of the uncertainties we assess for each parameter. The bases of the various input parameters are discussed in the respective subsections that follow.

**Geometry of Planar Normal Faulting**

We recognized the sparcity of data on the geometry of active normal faults for the Yucca Mountain region and decided to use data from studies of normal faulting earthquakes from other areas of the Basin-Range province as well as the focal mechanism data provided at the YMPHSA workshops by Ken Smith (1996, 1997) of the University of Nevada and the earlier research on the seismicity of southern Great Basin, including the Yucca Mountain area (Rogers *et al.*, 1991). We also studied the data of Doser and Smith (1989) who summarized the geometry of historic normal faults and used focal mechanism data for both short and long period arrivals, source mechanisms from seismic moments and from geologic and related geodetic information.

We also referred to published working models of large Basin and Range-type normal faulting earthquakes from Smith and Arabasz (1991). These include three of the largest earthquakes in the western U.S. that had dominantly normal-faulting slip: Ms 6.8 Dixie Valley, Nevada, earthquake of 1954; the Ms 7.5 Hebgen Lake, Montana, earthquake of 1959; and the Ms 7.3 Borah Peak, Idaho, earthquake of 1983.

The primary characteristics of these large earthquakes include rupture on planar normal faults, dipping 40° to 60°, nucleation at mid-crustal depths of about 15 km, and no evidence from the seismic data of non-planar geometries.

Estimates of fault dip are based on studies of the most modern (since 1954, when well-recorded seismic data became available) historical, scarp-forming nomal-faulting earthquakes as analogs. We chose 50°, 60° and 75° as our distribution of likely dips. Our rationale for these values is based on the minimum dip of 49° for one of the 1959 Hebgen Lake, Montana, main shock segments, including an error of 10°. We assigned 60° the greatest weight because this is a typical mid-value for the dips of earthquakes in the Basin and Range province (e.g., Doser and Smith, 1989, their Figure 4) and it is commonly measured surface dip throughout the province. It was determined using the most modern methodology and with the widest variety of instrumentation, short-and long-period data; several authors found a similar geometry (Richins *et al.*, 1985; Doser and Smith, 1985; Stein and Barrientios, 1985; Nablek *et al.*, Oregon State University, written communication, 1990). The upper bound value of 75° was used because it is considered a bound of the steepest dips of historical

earthquakes from seismic data, such as the 78±5° dip of the 1954 Rainbow Mountain, Nevada, earthquake. Also, this highest value is near that for steeper normal surface faulting of these normal-faulting events of approximately 90°. The estimates of dip are also closely constrained by field measurements made during mapping of Yucca Mountain and observations made from logging the ESF. Data from fault mechanism solutions for nearby earthquakes, notably from that of the 1992 Little Skull Mountain earthquake, also guided our estimates. Our observation, supported by regional data, is that steep dips measured in outcrop tend to decrease to moderate dips at seismogenic depths.

**Alternative Models**

We considered low angle and listric fault geometries as possible seismogenic structures. But because of the global lack of unequivocal data on focal mechanisms of large, scarp forming normal faulting earthquakes having dips less than ~40°, we did not consider the shallower fault dips for earthquake source at Yucca Mountain. That is not to say that low angle and listric faults do not exist in the Yucca Mountain region, but we consider that if they are present, they are not now seismogenic and were generated in an earlier tectonic regime. Hence, we do not appeal to detachment faulting as a tectonic model for fault behavior.

Fault width refers to the downdip dimension of a fault. Unless otherwise noted, we consider the width to be the seismogenic depth, taking into account the fault dip (i.e., the seismogenic depth divided by the sine of the fault dip).

**Magnitude versus fault length.** Estimating magnitudes on the basis of fault length is a conventional approach for all fault sources. Three lengths are estimated: the minimum, preferred, and maximum. Because many of the faults at Yucca Mountain are short relative to depth of the seismogenic crust, these lengths are considered to correspond to earthquake segments. Two regressions are used as scaling relations to estimate moment magnitudes: Mason (1996) and Wells and Coppersmith (1994). These relations are shown in Table SDO-2. Mason's relationship is based on earthquakes from extensional environments; Wells and Coppersmith (1994) use a worldwide data set of normal to oblique-slip earthquakes.

**Magnitude versus maximum surface displacement.** Because single-event surface displacements are available from the many trenches involved with this project, the

opportunity exists for estimating earthquake magnitude based on surface diplacement. Many of the displacements are small (less than a meter). Several trenches appear to be located such that the maximum surface displacement would have been recorded, but this is speculation, and local situations that would diminish surface rupture could prevail. There generally were only a few points of information along any one fault, and information commonly varied at each site. Only a few faults appeared to have documentable modes of rupture that might be inferred as average surface displacements. Many of the paleoevents at the sites have displacements of a few decimeters to a meter, and surface manifestation, after such rupture works its way through the volcanic carapace, may be attenuated up dip, broken up and discontinuous at the surface, and/or widely distributed between faults. Estimates of maximum surface displacement could be made and bracketed, however, using maximum single-event displacements from the trenches, or the maximum displacements for an event from different trenches. For distributed ruptures, displacements for the same event are added in a cross-strike manner to obtain a maximum surface displacement of the event.

As with fault length, two regressions are used to scale earthquake size as a function of displacement, one by Mason (1996), and one by Wells and Coppersmith (1994). These relations are shown in Table SDO-2. Mason's relationship is based on a data set using earthquakes from extensional envionments. Wells and Coppersmith use a worldwide data set. Mason's regression uses surface-wave magnitude, which is assumed to be equal to moment magnitude (see discussion in Wells and Coppersmith, 1994). Wells and Coppersmith's regression is in moment magnitude.

**Magnitude versus fault length x maximum surface displacement.** Mason (1996) developed a regression for magnitude versus fault length times maximum surface displacement, which provides a parameter that more closely estimates seismic moment than either of the base parameters individually. Both fault length and maximum surface displacement are determined as discussed above and simply are multiplied. Mason's regression uses surface-wave magnitude, which is assumed to be equal to moment magnitude (see discussion in Wells and Coppersmith, 1994).

**Magnitude versus fault area.** Fault area is estimated from two parameters, fault length and downdip width. Fault area also affords a closer estimate of seismic moment than does a

single parameter. However, the fault areas used in magnitude-scaling relationships typically are derived from aftershock data, so there is a large uncertainty in the resulting values. For example, many of the minimum downdip widths of faults are significantly limited by intersections with other faults. This limitation was added to the information constraining earthquake sizes by using the magnitude versus fault area relationship and by calculating seismic moments. Fault areas are calculated using the estimated fault lengths and downdip widths, and magnitudes are scaled using Wells and Coppersmith's (1994) regression, acknowledging the error produced by the lack of internal consistency (fault area versus aftershock area). Downdip widths were estimated considering maximum dynamic seismogenic depth, ranges in fault dips, and possible structural intersections.

**Magnitude versus length and slip rate.** Anderson *et al.* (1996) developed a magnitude-scaling relationship that includes fault slip rate and fault length. Their approach is based on observations that, for a given length, faults having lower slip rates or faults having longer recurrence intervals tend to have larger earthquakes. Although the method is controversial, it builds on the previously established observation that earthquake size has a dependency on earthquake return time (e.g., Kanamori and Allen, 1986) and tectonic environment (Scholz and Aviles, 1986). Wesnousky (1986) sorted magnitude versus fault length data into high and low slip-rate categories and regressed them separately to account for the potential effects on slip rate. Unfortunately, several of the faults in the Yucca Mountain area have slip rates lower than the data used in Anderson *et al.*; thus, the overall technique is given a third of the weight of other, more established, approaches.

**Magnitude versus seismic moment.** Seismic moments are estimated using fault area times average subsurface displacement times shear rigidity. Shear rigidity for the seismogenic zone is taken to be $3x10^{11}$ dynes/cm$^2$. Average subsurface displacements are considered to be half the maximum surface displacement. This ratio was chosen after examination of Figures 6 and 7 of Wells and Coppersmith (1994) and considerations that D.B. Slemmons articulated during the January 1997 Probabilistic Sesimic Hazards Analysis Workshop. Slemmons suggested that new studies will indicate that average subsurface displacements will be found to be about 38 percent of maximum surface displacements. Wells and Coppersmith (1994) find a mode of this ratio from 44 earthquakes to be 0.76. We use the rough average of these two ratios, 50 percent.

### 3.4.3 Recurrence

The assessment of earthquake recurrence for the local fault sources is based on the interpretation that all three types of rupture scenarios (individual ruptures, linked ruptures, and distributed ruptures) can occur. These data are interpreted to define the frequency of maximum events for each type of rupture behavior. The recurrence rates for "maximum" earthquakes are defined using the procedure described below. In constructing the recurrence relationships we follow the convention of Youngs *et al.* (1987) and consider that the maximum magnitude earthquake assessed above is the central estimate of a "characteristic" magnitude interval. For the characteristic and maximum moment recurrence models discussed below, the characteristic events are uniformly distributed in the magnitude range $M_{max}$±¼, such that the upper limit of the recurrence relationship is $M_{max}$+¼. For the exponential recurrence model the upper limit is also set at $M_{max}$+¼. Thus, the frequency of "maximum" earthquakes is interpreted to be the frequency of earthquakes of magnitude greater than or equal to $M_{max}$-¼. This frequency is interpreted to be the frequency of earthquakes within 1/2 magnitude unit of the maximum magnitude earthquake defined for each type of rupture behavior. For the individual fault rupture scenarios, the frequency of earthquakes smaller than the maximum magnitude minus 1/2 magnitude units are estimated using either a characteristic or truncated exponential recurrence model, weighted 0.7 and 0.3, respectively. Our preference for a characteristic model is based on the observation that paleoearthquake displacements exposed in the trenches at Yucca Mountain demonstrate repeated offsets of about a meter. However, we do not discount the observation that the historical seismicity of the southern Great Basin may have a truncated exponential distribution. The linked and distributed rupture scenarios are interpreted to be larger earthquakes that occur in addition to the individual rupture scenarios. Thus we allow for only these events to occur. As was the case for the regional sources, the size of earthquakes occurring on the local faults is limited to magnitudes of 6.2 and larger. The occurrence of smaller earthquakes is addressed by the regional source zones.

The relative frequency of each type of rupture behavior is estimated from the recorded paleoseismic data. If there have been $n$ paleoearthquakes on fault $x$, then we have $n$ observations of the fault's behavior. The number of times that it has ruptured as a single fault versus the number as a linked or distributed fault define the relative frequency of these types of behavior. Because of the uncertainty in assessing what type of behavior actually occurred

in each paleoevent, we assess the relative likelihood (or probability) of the various types of behavior that might have occurred for each event. Averaging these over all of the paleoevents provides an assessment of the expected relative frequency of each type of event. These relative frequencies are then multiplied by the overall frequency of events on the fault to define the actual frequency of occurrence of each type of behavior.

This type of analysis is motivated by the desire to incorporate as much of the extensive paleoseismic data set that has been developed at the Yucca Mountain site as possible. To be as clear as possible about this analysis, we have broken it up into steps, which are described individually in the following subsections, and an example is illustraded in Figure SDO-9. This analysis tracks earthquake occurrence rate (events/year) rather than recurrence intervals.

**Analysis step 1** determines the occurrence rates of earthquakes along the principal local faults. Three techniques were used to determine the occurrence rates for the faults, a moment rate technique, an average earthquake recurrence interval technique, and an average interseismic interval technique.

The moment rate technique uses the various fault lengths, down-dip widths, and slip rates to generate a moment rate ($MR = LWS\mu$, where MR = moment rate, L = length, W= downdip width, S = slip rate, and $\mu$ = shear rigidity [$3 \times 10^{11}$ dyne/cm$^2$]). Slip rates were determined using total offsets from trench logs and the estimated time since those offsets (S=O/T; S=slip rate, O = offset, T = time). Uncertainties in slip rates are calculated by cross multiplying the range in possible offset and dating uncertainties. The seismic moment was calculated using preferred values. Using the full range in moment estimations produced unreasonable results for occurrence rate. Thus, the maximum and minimum values were obtained by use of the preferred parameters, but considering the maximum and minimum displacement values. The seismic moment estimated for the fault is divided by the moment rate to obtain the recurrence interval for events. This interval is inverted to get occurrence rate.

The average earthquake recurrence interval technique is estimated by taking the age of the oldest reported paleoseismic event and dividing the age by the number of events that have occurred since, minus the most recent event. Since the elapsed time since the last event is an

incomplete interseismic interval, the last event and the time since the last event are removed from the calculation.

The average interseismic interval technique averages the preferred interseismic intervals determined for each fault. The maximum and minimum interseismic intervals are adopted directly for the maximum and minimum values. Five of the six principal faults have at least four or more paleoseismic events to consider for interseismic intervals. The other fault (the Iron Ridge fault) has two to three events.

In general the preferred values of the average and interseismic interval techniques are similar as we might expect. The most significant difference comes from the estimation of the maximum and minimum values. For the average earthquake recurrence interval technique, the uncertainty that is translated into maximum and minimum values is determined from the uncertainty in the age of the oldest event and the number of events since. The uncertainty in the interseismic interval technique comes from the variation of the interseismic intervals themselves.

These three estimates, moment rate, average recurrence interval, and interseismic interval, are averaged for estimating the occurrence rates ascribed to the fault. We weight these three methods equally because the uncertainty in the methods is roughly the same.

**Analysis step 2** is an empirical approach that uses data from the Yucca Mountain trenches to identify paleoseismic events. These are listed in Appendix SDO-2 for each fault, with a nominal age of each event listed as well. Then a single and perhaps multiple possible event histories are determined for a fault. If multiple possible event histories exist, the relative likelihood of these histories is assessed, and a relative weight is assigned to each history. For example, if there was uncertainty as to whether a particular paleoseismic event occurred, two models of paleoseismic history can be used, one with the uncertain event and one without.

**Analysis step 3**. Each paleoseismic event is considered an observation or sampling of a fault's behavior (whether it might behave as an individual, linked, or distributed fault during an earthquake event). Each paleoseismic event is considered an equally valuable piece of information, and is given a weight in the analysis of $1/n$, where $n$ is the number of

paleoevents in the history. This is not a "relative weight" in the classic sense; thus we call this a relative frequency. The series of paleoevents thus define the relative frequency of different rupture patterns.

**Analysis step 4** divides paleoseismic events into event scenarios and relatively weights these scenarios. Three main models of event scenarios are considered, (1) single fault, (2) linked faults, and (3) distributed faults. The potential event scenarios are determined considering potential correlations of events from trenching data on different faults and structural linkages.

Because of the small cross-strike distances, the highly interconnected nature of the faults, empirical information from historical Basin and Range province earthquakes, and the apparent similarities in age of paleoseismic events along different faults within the relatively small area of Yucca Mountain, we considered the occurrence of multiple fault scenarios to be a likelihood in some cases. The weighting between different event scenarios was based on the uncertainties in the age estimates of events, secondary correlation evidence (e.g., same volcanic ash found within the fault zone or in an event horizon), representations of event scenarios given in Chapter 5 of the Seismotectonic Framework report (USGS, written communication, 1996). Most of the weights are 50/50 or 30/70 between the single faults and multiple fault scenarios dependent on age uncertainties and number of correlating factors, or are equal weights across all event scenarios reflecting similar uncertainties in dates and high degrees of structural connectivity.

Earthquake lengths are based on the end-to-end length of the combined faults for the linked scenarios. Distributed fault scenarios involve parallel faults that fail together. For distributed scenarios, maximum surface displacements are combined in a cross-strike fashion, and lengths may or may not be increased over single fault scenarios. All events scenarios are presented in Appendix SDO-1 as a listing of all events, and under each of the six principal faults considered.

**Analysis step 5** calculates the occurrence rate of the event scenarios for each paleoseismic event. This is done by multiplying the occurrence rate from each fault times the relative weight of the paleoseismic histories times the relative frequency of a specific paleoseismic

event ($1/n$, where $n$ is the number of events) times the relative weighting of the specific event scenario (based on age uncertainties and structural connectivity).

**Analysis step 6** adds up the occurrence rates for each event scenario with that from multiple paleoseismic events along a fault. The occurrence rates for each event scenario involved in multiple paleoseismic events are added together. This now represents the occurrence rate of a specific scenario per fault. These results are displayed in the beginning of Appendix SDO-1 by principal fault. Note that there are different occurrence rates for some of the same event scenarios for different faults. These are resolved in the next step.

**Analysis step 7** combines the occurrence rates from event scenarios common to multiple principal faults. A simple averaging of the occurrence rates from different faults is done to accomplish this. These final values are the occurrence rates then used for the different event scenarios.

## 3.5 VOLCANIC SOURCES

Our team recognized the importance of volcanic-related seismicity in light of the Quaternary basaltic volcanoes near the Yucca Mountain site. We used the data from the Yucca Mountain volcanic hazard analysis (Geomatrix Consultants, written communication, 1996). We considered several sources that could be activated along the northeast alignment of approximately 1-million-year-old volcanic vents across Crater Flat, as well as those that might be associated with the Lathrop Wells vent at the south end of Crater Flat.

One volcanic source (Figure SDO-10) is taken to represent volcanism along the alignment of vents within an area determined by a spatial smoothing of the average distance between volcanic vents, that average defining a perimeter around each vent to make up a northeast-aligned source zone. We assumed two to three volcanic events per million years. The potential activity of this source was weighted 0.25.

Our second volcanic source is at the south end of the vent alignment that encompasses the 70,000-year-old Lathrop Wells volcanic vent (Figure SDO-10). We weighted the potential activity of that source 0.75.

The maximum magnitude for a volcanic earthquake was assigned on the basis of Smith and Jackson (1996), a study of volcanic-related earthquakes worldwide, as well as the recently completed Yucca Mountain Probabilistic Volcanic Hazard Assessment and its documentation (Probabilistic Hazard Analysis for Yucca Mountain, Nevada, Civilian Radioactive Waste Management System, Management and Operating Contract, BA00000-01717-2200-00082, Rev.0).

We characterize the distribution for volcanic-related earthquakes magnitudes as follows.

| Magnitude | Weight |
|---|---|
| $6.0 \pm 0.2$ | 0.1 |
| $5.8 \pm 0.4$ | 0.6 |
| $5.5 \pm 0.4$ | 0.3 |

Smith and Jackson (1996) found a maximum magnitude of M 4.5 for basaltic vents. We choose a preferred Mmax of 5.8 for volcanic source zones in the Yucca Mountain area on that basis, with the most likely occurrence along our northeast alignment.

# 4.0
# HISTORICAL SEISMICITY: EVALUATION AND TREATMENT OF RECORD PARAMETERS

## Spatial Smoothing

The final earthquake catalog data were treated by a smoothing algorithm as a means of distributing the seismic moment uniformly across the source zones.

Our smoothing parameters were choosing from three zones:

(a) Uniform smoothing with fixed boundaries of the source areas were chosen to approximate the long term windows (thousands to hundreds of thousands of years) that would encompass seismotectonic potential of our identified source areas.

Weight = 0.50

(b) We considered shorter time frames of tectonic processes (a few hundred years), we assigned a weight to Frankel's (1995) smoothing algorithm for a 10 km radius of the Gaussian kernel (with a 1 s standard error ) and with magnitude 3 and 5 cutoffs. This radius was assumed to take into account the events with a 10 km aftershock length that generally are consistent with a few tens to a few hundred year return period for the Basin-Range.

Weight =0.25

(c) We addressed a wider geographic window (several hundred years) by assigning a wider aperture of 20 km to Frankel's (1995) smoothing algorithm for the Gaussian kernel for a 1 s standard error for his radii specifications for magnitude 3 and 5 cutoffs. This considers aftershock distributions that correspond to larger and less frequent earthquakes of several hundred years for the Basin-Range.

Weight = 0.25

Alternate Model—We initially attempted to smooth the earthquake catalog data by developing a weighting algorithm that would have as its smoothing kernel a radius determined by first searching a grid up to 50 km, then assigning a window with a radius on the basis of the aftershock length vs. magnitude (using the relationship of Wells and Coppersmith, 1994). However, because of the low background historical seismicity of the Yucca Mountain area, this method produced a very small effective search radius of ~5 km or less and was not used.

**Relationships Between Magnitude Scales**

We studied the magnitude scales for various catalog contributions that were done by Woodward-Clyde Federal Services. After examining these conversions we chose to use them as described in the Woodward-Clyde Federal Services Yucca Mountain PHSA unpublished report (I. Wong, WCFS, written communication, 1996).

**Magnitude Uncertainties**

We assessed magnitude uncertainties by comparing the catalog period with the Woodward-Clyde Federal Services Yucca Mountain PHSA unpublished report on the Yucca Mountain composite catalog (I. Wong *et al.*, WCFS, written communication, 1996) as follows:

| Time Period | Estimate of Magnitude Uncertainty |
|---|---|
| 1900-1930 | ± 0.8 |
| 1931-1961 | ± 0.6 |
| 1962-1970 | ± 0.5 |
| 1971-1978 | ± 0.2 |
| 1978-present | ± 0.2 |

**Declustering Parameters**

We used a distribution for declustering of our earthquake catalog as follows.

(a) We used Youngs *et al.* (1987) declustering parameters (updated Geomatrix version 5) for the four weighting parameter sets.

Weight = 0.6

(b) We used the Veneziano and van Dyke (1985) approach but downweighted the method as it is not yet fully accepted. It used a variable radius-dependent spatial smoothing window to acquire sufficient numbers of earthquakes to determine if a single event was independent either in time or space to the previous event. Parameters are dynamic and not stationary over the study area.

Weight = 0.2

(c) Our team, SDO, also developed a modified time-distance window based upon Youngs *et al.* (1987) declustering parameters. These were patterned after the Wasatch Front seismicity and are as follows:

Weight = 0.2

| Mag. | Time (hours) | Distance (km) |
|---|---|---|
| 2.5 | 20 | 20 |
| 3.5 | 30 | 30 |
| 4.5 | 100 | 40 |
| 5.5 | 300 | 60 |
| 6.5 | 600 | 200 |
| 7.25 | 2000 | 300 |

## Catalog Completeness

Catalog completeness is a parameter that captures the idea of a minimum magnitude cutoff above which the earthquake catalog is complete such that a recurrence curve will not deviate from an exponential decay with an assumed constant slope. We estimated the completeness by examining the temporal distribution of earthquakes using the method of Stepp (1972) to each of the catalogs. Our team's estimate of the completeness from our own time-space windows are:

| Magnitude Completeness | Period |
|---|---|
| M 6+ | 1900 present |
| M 5.0 - 5.9 | 1924 present |
| M 4.0 - 4.9 | 1934 present |
| M 3.5 - 3.9 | 1950 present |
| M 3.0 - 3.5 | 1962 present |
| M 2.5 - 2.9 | 1972 present |
| M 2.0 - 2.4 | 1979 present |

The catalog completeness intervals for the catalogs declustered using the Youngs *et al.* (1987) and the Veneziano and van Dyke (1985) approaches are based on those presented by Ivan Wong in SSC Workshop 3 and on review of the data. The completeness intervals are:

| Completeness Magnitude | Period |
|---|---|
| M 7.0+ | 1880-present |
| M 6.0-6.9 | 1900-present |
| M 5.0-5.9 | 1914-present |
| M 4.0-4.9 | 1934-present |
| M 3.5-3.9 | 1961-present |
| M 2.5-3.5 | 1979-present |

Recurrence parameters were estimated using the maximum likelihood method described in Section 3.1 of the main report. The minimum magnitude was set at 2.0 except for Zone 2. For this zone, the minimum magnitude was set at 2.5 because the catalog appeared to be incomplete at magnitude 2.

# 5.0
# FAULT DISPLACEMENT

## 5.1 INTRODUCTION

In dealing with fault displacement hazard, our team considered that the level of our scientific knowledge of the subject and technique is less certain than that applicable to seismic source characterization. There are a number of reasons for this, but a prime consideration is that idealizations that can be applied to rock behavior at seismogenic depth are not as readily applicable to the upper one or two kilometers of the earth's crust where the repository site is located. At seismogenic depths (~ 4 to 19 km) rock is under high confining stress and is assumed to behave as an elastic, isotropic medium; the strength of fractures is high ($0.6 < \mu < 0.8$) and exhibits essentially frictional behavior. At depths less than about 4 km the crustal carapace consists of a variety of rock types ranging from pristine rock, to weathered or altered rock, to consolidated and unconsolidated alluvium; here, fracture strength may be appreciably different than the shear strength of the host material.

Because of these differences in properties and conditions, strain release (stress drop) considered as seismogenic slip along deep-seated faults may not efficiently be propagated to the surface as a fault displacement. Accordingly, we followed closely working models and data presented at the Yucca Mountain Fault Displacement workshops that extend our teams concept of the problem, and gave weight to the cogency and reasoning of alternate approaches. Our basic premise, however, was to use, where possible, observational data on principal and distributed faulting appropriate for the Basin and Range extensional regime, and especially to use data from the Yucca Mountain area. This is not to say that the problems of fault displacement are not amenable to epistemic solution, though we emphasize that uncertainties in the interpretation of the data may be large. We also note that it is important to the user of our characterization to understand that we downplayed research-oriented approaches and attempted to understand the uncertainties of observational data, and hence dealt with them in a probabilistic sense.

There are three major questions that we considered:

First, there is the problem of what constitutes principal surface displacement. Ideally, principal surface displacement is systematically proportional to the source-depth displacement of the causative earthquake. In practice, the primary displacement is smaller to a greater or lesser degree for the following reasons:

- Anti-clustering and roll-over effects in the hanging wall.
- Material and fault damage differences in hanging wall versus foot wall.
- Strain diffusion associated with local fracturing, reconsolidation, and fissuring.

Second, there is the complication of secondary faulting: How can we discriminate secondary from primary faulting on a genetic basis?

- Time-dependent strain release involves reconsolidation, compaction, groundwater phenomena, foot-wall degradations, subsidence, stress history, "effective elastic thickness" phenomena, etc. These factors contribute to well-defined criteria for defining the extant of these ruptures.

Third, there is a time and spatial sampling problem.

- Degradation of sample sites with time.
- Sample technique: authoritative vs. random/systematic sampling.

To address these problems we approached the analysis at two levels: one for ruptures on the primary faults, i.e., those considered to be seismogenic (at depth), and one for distributed rupturing on secondary faults (near the ground surface). There is a general logic tree for each. The methodology for displacement along the seismogenic faults is largely an extension of our teams (SDO) approach to the seismic source characterization analysis, using the magnitudes of earthquakes and their frequency of occurrence developed in Sections 3 and 4. We considered distributed or secondary displacements to be diffusely scattered and discontinuous ruptures that mostly occur in the hanging wall of normal-slip faults. These are interpreted to result from local strain release distributed along and across the hanging wall, triggered by a nearby earthquake or by non-tectonic mechanisms such as thermal contraction, ground slumping, localized ground subsidence due to ground water withdrawal, etc.

Most of the methods we used for estimating the potential for distributed faulting lack the refinement of seismic source characterization. However, we considered them reasonable

given the relatively small data base, the precision of the data, the generally limited knowledge of the normal faulting process and the relationships of primary to secondary fault triggering. To span the variety of methodologies, we used several approaches that we judged applicable to the Yucca Mountain environment to overcome the large uncertainties or potential bias of any one approach.

## 5.2 PRINCIPAL FAULTING DISPLACEMENT CHARACTERIZATION

The logic tree for characterizing the potential for principal fault displacement (Figure SDO-11) is divided into five parts: (1) type of event, (2) frequency of occurrence of events, (3) approach for estimating fault displacement, (4) scaling techniques, and (5) distribution for displacement at a point. The following discussion expands these topics.

### 5.2.1 Type of Event

We considered two levels of principal rupture size along seismogenic faults: maximum displacement events and events smaller than the maximum earthquake. The characterization of displacement hazard from events associated with distributed displacements is described in Section 5.3. Defining the size and frequency of maximum earthquakes (those within ½ magnitude unit of the upper bound earthquake for the fault) are a focus of the earthquake source characterization for assessment of ground motion hazard. The frequency and size distribution of smaller earthquakes down to the maximum background earthquake are assessed using the earthquake recurrence models described in Sections 3.0 and 4.0 We consider that secondary displacement is possible in response to earthquakes along other faults, including aftershock sequences. The characterization of these faults is discussed in Section 5.3. In that part of the analysis, the seismogenic fault is treated in the distributed faulting as the larger end of the fractal distribution of faults.

### 5.2.2 Frequency of Occurrence of Principal Faulting Events

We utilize the earthquake approach for characterizing principal faulting displacement hazard. The frequency of earthquakes along the seismogenic faults is developed in our (team SDO) earthquake source characterization study (Sections 3 and 4). This is based on three approaches: (1) averaging of moment rates; (2) using an average recurrence interval; and (3) using the interseismic time interval. Events that have magnitudes distributed between the maximum earthquake and the maximum background earthquake have their occurrence rates

developed using the characteristic and truncated exponential models. These models are weighted 0.7 and 0.3, respectively.

The probability of seismogenic rupture at or near the surface is computed using an empirical relationship between the probability of surface rupture and earthquake magnitude developed from data presented by S. K. Pezzopane and T. E. Dawson (USGS, written communication, 1996). Figure SDO-12 shows the results of fitting a logistic probability model to the data sets presented by S. K. Pezzopane and T. E. Dawson (USGS, written communication, 1996) for recent Basin and Range earthquakes (see Appendix H, Section H.4.1). We assign equal weight to these two treatments. The probability of surface rupture at any given point along a fault is computed by randomizing the location of the rupture along the length of the fault.

### 5.2.3 Approach for Estimating Fault Displacement

The approaches used for estimating fault displacement include empirical regressions of observations of faults that produce normal-faulting earthquakes, data from single-event paleoearthquake displacements, and an along-strike displacement plot for the Solitario Canyon fault determined by Allan Ramelli (Nevada Bureau of Mines and Geology, written communication, 1997) as part of the Yucca Mt. earthquake hazard assessment.

Four types of empirical regressions are used: (1) average displacement versus moment magnitude; (2) average displacement versus length; (3) maximum surface displacement versus moment magnitude; and (4) maximum surface displacement versus length. These are taken from Wells and Coppersmith (1994) and an analysis by the AAR Team of Yucca Mountain data. Both the average and maximum surface displacements are considered because both can be used for assessing the distribution for displacement at a point in an event.

Fault parameter data were taken from the trenching studies of Quaternary faults in the Yucca Mountain area and are the interpreted maximum surface displacements that have been reported in the earthquake seismic source characterization analysis. Average surface displacements were scaled from maximum surface displacements using scaling relationships of Wells and Coppersmith (1994) judged appropriate for an extensional, normal faulting stress regime. Wells and Coppersmith's (1994) Figure 5 plots the ratio of average surface

displacement to maximum surface displacement and shows a distribution between 0.2 and 0.8. We used the approximate average value of these data and take the ratio between average and maximum displacement to be 0.5.

The Ramelli fault displacement data for the Solitario Canyon fault is a combination of trench observations and measurements from the scarp observed along the Solitario Canyon fault trace (Figure SDO-13). It shows some of the ambiguities involved in assessing surface data from both random (field reconnaissance) and authoritative sampling (trench measurements). The curve is useful, however, because it uses direct information from the fault that is in close proximity to the Yucca Mountain site and therefore judged as a good proxy for conditions at the repository.

**5.2.3.1 Scaling Techniques.** The scaling techniques we used (Table SDO-6) are the regressions aforementioned and a theoretical relationship presented at the SSC workshop #4 and based on a rock mechanics approach (see Bruhn, 1997, SSC Workshop #5). The Wells and Coppersmith (1994) regressions are those for normal faults; the analysis by the AAR Team (presented at SSC workshop #4, Jan. 8, 1997) is developed using data from the Yucca Mountain area. Values from these regressions were used to scale the displacement diagrams presented in the next section.

**5.2.3.2 Distributions for Displacement at a Point.** Because engineered structures are designed for site specific locations, we need to be able to estimate the potential scale of local fault displacement. Typically, displacement at a surface rupture can range from large values along a single scarp, to smaller values across a broader stepped-scarp distribution. We attempt to model the distribution for the amount of displacement that occurs at a point on a principal rupture by employing a variety of displacement distributions (some named after their developers): (1) a compilation of five large Basin and Range historical earthquakes compiled by Wheeler (1989), called here the five-earthquake curves (Figure SDO-14),;(2) a fault-roughness curve (Figure SDO-15) which is developed in more of a rock mechanics sense by R. Bruhn; (3) a Yucca Mountain site-specific, trench-displacement distribution developed by the DFS Team (Figure SDO-16); and (4) for the Solitario Canyon fault, the displacement plot (Figure SDO-13) developed by Alan Ramelli of the Nevada Geological Survey.

The Wheeler five-earthquake curves (presented at SSC Workshop #5, April 15, 1997) are based on data from five large, scarp-forming Basin and Range province earthquakes. The ASM Team smoothed the data presented in Wheeler (1989) to derive, symmetric curves that define the median and range of the ratio of displacement at a point to the maximum displacement associated with an earthquake, *D/MD*, as a function of location along the principal fault rupture (Figure SDO-14). The Facilitation team developed a statistical model to represent this distribution (see Appendix H, Section H.3.1). The fault roughness curve is based on the consideration that surface roughness along a fault plane is related to amount of displacement, as noted by Ronald Bruhn (SSC Workshop #5). The SBK Team developed a model that represents the theoretical surface roughness along a fault and predicts a distribution for the ratio of displacement at a point to the maximum displacement associated with earthquake magnitude (Figure SDO-15). This distribution is analogous to the empirical distribution developed by the ASM Team (Figure SDO-14) and presented at SSC Workshop # 5, April 15, 1997. Although Bruhn's model is considered to portray real displacement variation along strike, we note that it is an untested theoretical model and should be weighted accordingly. The Facilitation team developed a statistical model to represent this distribution (see Appendix H, Section H.3.2).

The Yucca Mountain trench-displacement distribution, developed by the DFS Team and presented at SSC Workshop # 5, April 15, 1997, examines the event-to-event variability in displacement at a point on a fault about the average historical displacement (Figure SDO-16). This distribution was originally specified as a triangular distribution by the DFS team. However, the Facilitation team determined that a gamma distribution provided a better fit to the data (see Appendix H, Section H.2.1) and we adopt that distribution.

The longitudinal displacement profile for the Solitario Canyon fault offered by Ramelli (Figure SDO-13) shows a large "bump" in fault displacement created entirely by measured offsets in trenches T1 and T8. Elsewhere along the fault, displacement determined by trenching is compatible with scarp heights. Why are the T1 and T8 offsets on the fault anomalously large? The answer seems to be fault segmentation (Ramelli, SSC Workshop #5 information transmittal, May 5, 1997). But we are cautious when asked to compare scarp heights cited by Simonds *et al.* (1995) from field reconnaissance with displacements

measured in four trenches. Two of the trenches, T1 and T3, give displacement values that are twice as great as the range of all other measurements. This leads us to ask what is actually being measured in these two trenches that returns such anomalously large mid- to late-Quaternary displacements? If we project a line through the span of displacements of all the other data sources we get a broad convex longitudinal profile along the fault, a curve similar to that obtained by Jim Yount (SSC Workshop # 6, June 1, 1997), who measured cumulative displacement with reference to a single Miocene horizon the observed length of the fault.

**5.2.3.3 Assessment of the Distribution for Amount of Displacement at a Point on a Principal Rupture.** The procedures to assess the distribution of potential amount of displacement at a point are shown on Figure SDO-11. There are two approaches: one based on assessment of the maximum displacement, *MD*, associated with an earthquake; and one based on an assessment of the average surface displacement, *AD*, that occurs during an earthquake. These two approaches are given equal weight in the analysis because of the uncertainties we describe in the Introduction.

The estimation of *MD* and *AD* depends upon the size of the earthquake. For magnitudes smaller than $m^U$- ½ the estimation is based solely on the relationships given in Table SDO-6 for *MD* and *AD* as a function of earthquake magnitude. For the maximum events ($m^U$- ½ ≤ $m$ ≤ $m^U$), we also estimate *MD* and *AD* using scaling relationships based on the assessment of rupture length using the relationships in Table SDO-6, and directly from the paleoseismic data. The weights assigned to these various approaches are 0.2 to assessment based on magnitude, 0.4 to assessments based on rupture length, and 0.4 on the paleoseismic displacement data. These weights reflect the relative importance we place on empirical data. For assessment of *AD* as a function of rupture length, equal weight is given to the Wells and Coppersmith (1994) regression and the regression developed by the AAR team (Table SDO-6).

The displacement plot for the Solitario Canyon fault (Figure SDO-13) allowed us to consider a different treatment for displacement along this fault. The displacement at any point of interest is read from the displacement curve and is taken to be the average displacement at that point during maximum earthquakes. This estimate is given a weight of 0.7 and all of the above assessments are given a combined weight of 0.3. We have not been able to determine

whether the displacement peak along the Solitario Canyon fault is a segmentation phenomenon or a sampling alias; we consider the data with due caution, in light of possible interpretations that may significantly bias analytical conclusions.

Given an assessment of *MD* from the various scaling relationships, the probability of exceeding a specified displacement at a point is computed as follows: The uncertainty in MD in a single event is considered to be lognormally distributed about the assessed value, with a standard deviation of log (*MD*) equal to that obtained by Wells and Coppersmith (1994) from regression analysis of empirical data. This lognormal distribution is used to assess the value of *MD* in a single earthquake. Given *MD* for an individual earthquake, the probability of exceeding a specified displacement is computed using the distributions for *D/MD* shown on Figures SDO-14 and SDO-15. The empirical distribution developed by the ASM team (Figure SDO-14) is weighted 0.8 and the theoretical distribution developed by the SBK team (Figure SDO-15) is weighted 0.2 for the reasons discussed above in Section 5.2.3.2.

Given an assessment of *AD*, the probability of exceeding a specified displacement at a point is computed as follows. The estimate of *AD* is considered to represent the average displacement over multiple earthquakes. The distribution for the ratio of the displacement in a single event to the average over multiple events, *D/AD*, developed by the Facilitation team from the data presented by the DFS team (Figure SDO-16), is used to assess the probability of exceeding a specified displacement.

## 5.3 DISTRIBUTED FAULTING DISPLACEMENT CHARACTERIZATION

Modeling the potential displacements from distributed faulting involves: (1) evaluating the characteristics of faults not directly part of the primary fault trace; (2) estimating the cumulative magnitude of the distributed fault displacements and the probability of occurrence of subsequent displacements; and (3) evaluating the affect of the free surface on fault propagation from the repository depth to the surface. Figure SDO-7 shows the logic structure used to characterize distributed faulting hazard. Two approaches were used. One is based on assessment of the frequency at which earthquakes on the various seismic sources induce distributed slip on the feature of interest. This is termed the earthquake approach. The second approach uses the cumulative slip at the point of interest to estimate the slip rate and displacement per event. This is termed the displacement approach. Both approaches are

used for features that are subject to only distributed faulting hazard, with the earthquake approach given a weight of 0.8 and the displacement approach given a weight of 0.2. The earthquake approach is given a higher weight because it has a stronger theoretical basis and a more complete database. It is also favored because it is ties to our paleoearthquake analysis. The displacement approach has not been studied in as much detail and has limited data. For those features that are also subject to principal faulting hazard, only the earthquake approach is used. Again, the large uncertainties associated with near-surface phenomena and widely variable material properties of media in the upper few hundred meters lead us to give a relatively low weight to the displacement approach.

### 5.3.1 Earthquake Approach to Distributed Faulting Hazard

The steps in the earthquake approach are: (1) assessment of the probability that distributed faulting can occur on the feature (activation probability); (2) an assessment of the probability of slip in an individual earthquake; and (3) an assessment of the distribution relative to the amount of potential total displacement.

**5.3.1.1 Activation Probability.** The probability that an individual fault can be activated among many during a distributed faulting event is estimated using an analysis of slip tendency of faults with respect to the regional stress field (Morris *et al.*, 1996). The slip tendency technique considers the ratio of shear to normal stresses imposed on a fault within a regional stress field. Slip tendency, $T_S$, reduces to $\mu$, the coefficient of static friction which, according to Byerlee's law (Byerlee, 1978), is 0.85 from ground surface to seismogenic depths (10 km). H. L. McKague *et al.* (CNWRA, written communication, 1996) present an analysis of the slip tendency of faults in the Yucca Mountain region. Their analysis of the local faults (their Figure 3-5b) indicates the north-south trending faults have the highest slip tendency (~0.7). Because most of the larger north-south trending faults show evidence of Quaternary slip, we utilize a value of $T_S$ of 0.7 to correspond to a probability that slip can occur, $P(C)$ of 1.0. For faults and features with other orientations, we define $P(C)$ as the ratio $T_S$ /0.7. For northwest-southeast trending structures, $T_S$ read from Figure 3-5b of H. L. McKague *et al.* (CNWRA, written communication, 1996) is approximately 0.55, resulting in $P(C) = 0.8$.

**5.3.1.2 Probability of Slip Per Event.** The frequency of occurrence of earthquakes on each of the seismic sources is defined by our seismic source characterization described in Sections 3.0 and 4.0. The probability of distributed slip on a feature in an individual earthquake is assessed using an analysis of the density of distributed rupture based on the mapped patterns of rupture presented in S. K. Pezzopane and T. E. Dawson (USGS, written communication, 1996). The logistic regression model presented by R. R. Youngs (Yucca Mountain SSC Workshop #6) was adopted (Figure SDO-18) (see also Appendix H, Section H.4.2). We excluded the data for hanging wall cracking from the 1988 Chalfant Valley earthquake and data from the 1980 Mammoth earthquake because these earthquakes are considered background type earthquakes. The curves show the probability of secondary rupture occurring at a point as a function of earthquake magnitude, distance from the principal rupture, and location in the hanging wall or foot wall of the rupture. For earthquakes occurring on the regional areal source, it is considered equally likely that the point of interest lies in either the hanging wall or the foot wall of the rupture.

We further modify the probability of distributed rupture in an event by a factor related to the orientation of the feature relative to the principal fault rupture. The distribution of the orientation of distributed ruptures with respect to the principal rupture provides an assessment of the likelihood that distributed faulting occurs on a feature with a given orientation with respect to the strike of the earthquake-generating fault. Maps of historical ruptures presented in S. K. Pezzopane and T. E. Dawson (USGS, written communication, 1996) were used to assess the relative frequency of distributed ruptures in increments of 5° of the angle $\theta$ between the strike of the principal rupture and the strike of the distributed rupture (see Appendix H, Section H.4.3). This relative frequency was used to define the likelihood of rupture as a function of relative strike between the principal rupture and the feature of interest. We selected the assessment based on a minimum of three points defining the distributed rupture trace because the process used to digitize the fault maps produced a distribution of two-point rupture traces with modes in the north-south and east-west directions, suggesting poor estimation of the strike azimuth distribution.

The strike azimuth for earthquakes occurring in the regional source zone is not known. Examination of the orientation of nodal planes of Yucca Mountain region earthquakes presented in Chapter 7 of USGS (written communication, 1996) indicates a nearly random

pattern. Therefore, we assume that the strike azimuth of these earthquakes is uniformly distributed from 0° to 360° and compute an average value of the orientation probability of 0.34 to apply to these earthquakes.

**5.3.1.3 Probability Distribution for Displacement at a Point.** Two approaches are used to assess the distribution of possible displacements at a given point along a fault scarp induced by slip on an earthquake source: one based on the ratio of cumulative displacements; and one based on maximum potential displacement computed from earthquake magnitude.

**Cumulative Displacement Ratio Approach.** In this approach, we consider the ratio of displacement on the principal rupture to displacement on the secondary rupture to be equal to the ratio of their cumulative displacements. We define a factor, *RF*, that is used to scale the principal rupture displacement to the distributed rupture displacement. The scaling factor *RF* is set equal to the ratio of the cumulative displacement on the fault of interest to the cumulative displacement on the earthquake source fault. We impose an upper limit of 0.8 to *RF* based on the maximum ratio of secondary to primary slip reported by Coppersmith and Youngs (1992). The procedures described in Section 5.2.3.3 are used to assess the distribution for slip on the principal rupture at its closest approach and this slip is scaled by *RF* to the point of interest. This approach is given a weight of 0.2. The low weight takes into account the uncertainties associated with origin, mechanics, displacements, and slip histories of shallow distributed faults compared to the seismogenic faults.

The application of this approach requires an assessment of the average cumulative displacement for each of the seismic sources in the vicinity of Yucca Mountain. The assessed values are:

| Source | Average Cumulative Displacement (m) |
|---|---|
| Paintbrush Canyon | 380 |
| Bow Ridge | 244 |
| Solitario Canyon | 457 |
| Fatigue Wash | 396 |
| Windy Wash | 380 |
| N. Crater Flat | 244 |
| S. Crater Flat | <244 |
| Iron Ridge | 350 |
| Stagecoach Road | 457 |
| Bare Mountain | 500-900 |

When simultaneous fault ruptures are considered, the largest cumulative displacement among the individual faults is used to define *RF*.

**Displacement Potential Approach.** As an empirical data set, secondary (or distributed) faults include numerous, difficult to discriminate strain phenomena along with true fault displacements. We consider that distributed displacement represents an upper limit of stain, i.e., failure in the rock mechanics sense, but that all the strain effects measurable as geodetic displacement normal to the rupture are consequences of main fault plane seismogenic rupture. The displacement potential approach simply acknowledges the reality that surficial materials are not classic elastic media and cannot be expected to behave (strain and fail) the same way a seismogenic fault does at depth.

For this approach we used a distribution ratio of secondary to primary slip empirically observed in historical, ground-breaking earthquakes in the Basin and Range province: (1) the **M** 7.1 1954 Fairview Peak, Nevada, earthquake and associated Stingaree Valley rupture; (2) the $M_s$ 7.5 1959, Hebgen Lake, Montana, earthquake; and (3) the $M_s$ 7.3 1983 Borah Peak earthquakes recognizing there are many more data points in the hanging wall than in the foot wall. Figure SDO-19 shows maximum distributed fault displacements normalized to the maximum principal fault rupture, *MD*, plotted versus distance from the principal rupture, and distinguishes displacement in the hanging wall from the foot wall side of the fault. We define an approximate envelope of the observed data on the hanging wall side of the rupture and fit an exponential curve to these data, as shown on Figure SDO-19. An exponential

curve is used because it is a simple parametric model that allows for a gradual decay of amplitude with distance. The resulting curve for the hanging wall displacement potential is

$$D(\text{distributed in hanging wall})/MD(\text{principal}) = 0.35 \times \exp(-0.091r)$$

where $r$ is the distance from the principal rupture. Examination of data presented in S. K. Pezzopane and T. E. Dawson (USGS, written communication, 1996) and Coppersmith and Youngs (1992) indicates that the distributed faulting zones on the foot wall side of normal fault ruptures are much narrower that those on the hanging wall side of the rupture. Consequently, we assume that the rate of decay of distributed displacement amplitude is 50 percent greater on the foot wall side than on the hanging wall side, and using the single foot wall data point define a foot wall displacement potential as:

$$D(\text{distributed in foot wall})/MD(\text{principal}) = 0.16 \times \exp(-0.137r)$$

The displacement potential is interpreted to represent the 95$^{th}$-percentile of the distribution of possible displacements, with the lower limit of this distribution equal to 0. We use a distribution with a similar degree of skewness as exhibited by the distribution for *D/AD* shown on Figure SDO-16 and impose an upper limit to the displacement potential equal to the cumulative displacement on the feature. As described in Appendix H, the various normalized displacement data sets developed by the expert teams can be modeled by gamma distributions with the shape parameter, $a$, of about 2.5. For $a = 2.5$, the 95 $^{th}$-percentile of a gamma distribution occurs at $5.535b$, where $b$ is the normalizing parameter of the distribution. Thus, we define a gamma distribution for the distribution of $D$(distributed)/$MD$(principal) at a distance $r$ from a principal rupture with $a$ equal to 2.5 and $b$ equal to the displacement potential defined by the above relationships divided by 5.535. The computation of the distribution for the displacement is completed by utilizing a lognormal distribution for *MD* on the principal rupture about the values given by the various scaling relationships defined in Section 5.2.3.1.

We weight the displacement potential approach 0.8. In assessing the potential for fault displacement from earthquakes occurring in the areal source zone only the displacement

potential approach can be used because the cumulative displacement on the earthquake source is not known.

### 5.3.2 Displacement Approach to Distributed Faulting Hazard

The steps in the displacement approach are: (1) assessment of the probability that distributed faulting can occur on a fault (activation probability); (2) assessment of the rate of slip on the feature; (3) assessment of the average slip per event; and (4) assessment of the distribution for the amount of displacement. In the displacement approach the location, size, and orientation of the faults that generate earthquakes inducing the distributed slip are unknown.

**5.3.2.1 Activation Probability.** The probability that an individual fault can be activated during a distributed faulting event is estimated using the analysis of slip tendency of faults with respect to the regional stress field, as discussed in Section 5.3.1.1.

**5.3.2.2 Assessment of Slip Rate.** The Quaternary slip rate on the feature of interest is assessed by estimating the fraction of the cumulative slip that has occurred in the past 1.6 Ma, and dividing that slip by 1.6 Ma. Based on review of the various proposed slip histories for the Yucca Mountain faults, the following distribution is assessed for the percentage of cumulative slip that has occurred in the Quaternary, 0.2% (0.3), 0.6% (0.4), 2% (0.3).

**5.3.2.3 Assessment of Average Displacement per Event.** We utilize two approaches for estimating the average slip per event, $\bar{D}_E$. The first is based on the scaling relationships between cumulative offset and average offset developed by the AAR Team (SSC Workshop # 4, Jan. 8, 1997). The second is based on an analysis of the fault offset data from Yucca Mountain normalized by the cumulative offset on the fault. This empirical distribution was developed by the SBK Team (SSC Workshop #6, June 1, 1997) (see Figure SDO-20). These two alternatives are given equal weight. The frequency of faulting events is equal to the fault slip rate divided by the average slip per event.

**5.3.2.4 Distribution for Displacement at a Point.** The approach for assessing the distribution for the displacement in an event is tied to the approach used for estimating the average slip per event. If the AAR scaling relationships are used, then the exponential distribution for $D/MD^{max}$ developed by AAR is used to calculate the probability distribution

for $D$, with $MD^{max} = \bar{D}_E$ /0.83 based on the scaling relationship developed by the AAR team. If the approach developed by the SBK team is used, then the empirical distribution shown on Figure SDO-20 is used to assess the probability distribution for displacement. This distribution was modeled by the Facilitation team by a gamma distribution (see Appendix H, Section H.2.6).

## 5.4 DATA FOR NINE CALCULATION SITES

The following summarizes the data required to characterize the displacement hazard at each of the nine demonstration sites.

### Point 1 Bow Ridge fault

Site of potential principal faulting , use the methods described in Sections 5.2 and 5.3.1. For distributed faulting , P(C) = 1.0. The paleoseismic $MD$ = 44 cm, with assumed lognormal distribution, and $\sigma_{\log(MD)}$ = 0.42 based on empirical models. The assessed cumulative displacement at Point 1 is 200 m. The distribution for the length of the feature is {7 (0.3), 8 (0.4), 10 (0.3)} km.

### Point 2 Solitario Canyon fault

Site of potential principal faulting , use the methods described in Sections 5.2 and 5.3.1. For distributed faulting , P(C) = 1.0. The paleoseismic $MD$ = 0.7 m, with assumed lognormal distribution, and $\sigma_{\log(MD)}$ = 0.42 based on empirical models. The paleoseismic $AD$ estimated from the profile developed by Alan Ramelli is 25 cm. The assessed cumulative displacement at Point 2 is 700 m. The distribution for the length of the feature is {16 (0.3), 18.5 (0.4), 21.5 (0.3)} km

### Point 3 Drill Hole Wash fault

Site of distributed faulting, use the methods described in Section 5.3. $P(C)$ = 0.8 from slip tendency. The cumulative displacement is assessed to be 12 m.

### Point 4 Ghost Dance fault

Site of distributed faulting, use the methods described in Section 5.3. $P(C)$ = 1.0 from slip tendency. The cumulative displacement is assessed to be 40 m.

**Point 5 Sundance fault**

Site of distributed faulting , use the methods described in Section 5.3. $P(C) = 0.8$ from slip tendency. The cumulative displacement is assessed to be 11 m.

**Point 6 Unnamed fault west of Dune Wash**

Site of distributed faulting , use the methods described in Section 5.3. $P(C) = 1.0$ from slip tendency. The cumulative displacement is assessed to be 150 m.

**Point 7 Point 100 m east of Solitario Canyon**

Site of distributed faulting, use the methods described in Section 5.3. For point 7a, $P(C) = 1.0$ from slip tendency and the cumulative displacement is 2 m. For point 7b, $P(C) = 1.0$ from slip tendency and the cumulative displacement is 10 cm. It is judged that the probability of displacement in intact rock (point 7d) is essentially negligible because the Yucca Mountain block is highly faulted and fractured at a wide range of scales and displacement within the block will likely occur along these pre-existing zones of weakness rather than break intact rock. Fractures with no displacement (point7c) are either small features or are on the fringe of a larger feature. In both cases, secondary displacement will probably be negligible.

**Point 8 Point midway between Ghost Dance and Solitario Canyon faults**

Use the same set of parameters defined above for Point 7.

**Point 9 Midway Valley**

Site of distributed faulting , use the methods described in Section 5.3. $P(C) = 1.0$ from slip tendency. The cumulative displacement is assessed to be 50 m.

# 6.0
# REFERENCES


Anderson, J.G., Wesnousky, S.G., and Stirling, M.W., 1996, Earthquake size as a function of fault slip rate: Bulletin of the Seismological Society of America, v. 86, n. 3, p. 683-690.

Anderson, R.E., Bucknam, R.C., Crone, A.J., Haller, K M., Machette, M.N., Personius, S.F., Barnhard, T.P., Cecil, M.J., and Dart, R.L., 1995b, Characterization of Quaternary and suspected Quaternary faults, regional studies, Nevada and California: U. S. Geological Survey Open-File Report 95-599, 56 p.

Anderson, R.E., Crone, A.J., Machette, M.N., Bradley, L.-A., and Diehl, S.F., 1995a, Characterization of Quaternary and suspected Quaternary faults, Amargosa area, Nevada and California: U. S. Geological Survey Open-File Report 95-613, 41 p.

Brocher, T.M., Carr, M.D., Fox, K.F., J., and Hart, P.E., 1993, Seismic reflection profiling across Tertiary extensional structures in the eastern Amargosa Desert, southern Nevada, Basin and Range province: Geological Society of America Bulletin, v. 105, p. 30-46.

Brocher, T.M., Hart, P.E., Hunter, W.C., and Langenheim, V.E., 1996, Hybrid-source seismic reflection profiling across Yucca Mountain, Nevada: regional lines 2 and 3: , U.S. Geological Survey Open-File Report 96-28, 110 p.

Brocher, T.M., and Hunter, W.C., 1996, Seismic reflection evidence against a shallow detachment beneath Yucca Mountain, Nevada: High-Level Radioactive Waste Management Proceedings of the Seventh International Conference, Las Vegas, Nevada, American Nuclear Society, La Grange Park, Illinois, p. 148-150.

Brun, J.-P., Sokoutis, D., and Van Den Driessche, J., 1994, Analogue modeling of detachment fault systems and core complexes: Geology, v. 22, p. 319-322.

Burchfiel, B.C., Hodges, D.V., and Royden, L.M., 1987, Geology of Panamint Valley-Saline Valley pull apart system, California; palinspastic evidence for low-angle geometry of a Neogene range-bounding fault: Journal of Geophysical Research, v. 92, p. 10,422-10,426.

Byerlee, J. D., 1978, Friction of rocks: Pure and Applied Geophysics, v. 116, p. 615-626.

Carr, W. J., 1984, Regional structural setting of Yucca Mountain, southwestern Nevada, and late Cenozoic rates of tectonic activity in part of the southwestern Great Basin, Nevada and California: U.S. Geological Survey Open-File Report 84-854, 109 p.

Carr, W.J., 1988, Volcano-tectonic setting of Yucca Mountain and Crater Flat, southwestern Nevada: U.S. Geological Survey Bulletin 1790, p. 35-85.

Carr, W.J., 1990, Styles of extension in the Nevada Test Site region, southern Walker Lane Belt; an integration of volcano-tectonic and detachment fault models, *in* Wernicke, B. P., ed., Basin and Range extensional tectonics near the latitude of Las Vegas, Nevada: Geological Society of America Memoir 176, p. 283-303.

Castro, G., and Poulos, S., 1977, Factors affecting liquefaction and cyclic mobility: American Society of Civil Engineers, Journal of the Geotechnical Engineering Division, v. 103, n. GT6, p. 501-516.

Coppersmith, K.J., and Youngs, R.R., 1992, Earthquakes and tectonics: in McGuire, R.K., ed., Demonstration of a Risk-Based Approach to High-Level Waste Repository Evaluation: Phase 2, Electric Power Research Institute, EPRI TR-100384, Palo Alto, California

Cornwall, H.R., 1972, Geology and mineral deposits of southern Nye County, Nevada: Nevada Bureau of Mines and Geology, Bulletin 77, 49 p.

Cowie, P. A., and Scholz, C.H. 1992, Growth of faults by accumulation of seismic slip: Journal of Geophysical Research, v. 97, p. 11085-11095.

Decker, P.L., 1990, Style and mechanics of liquefaction-related deformation, lower Absaroka Volcanic Supergroup (Eocene), Wyoming: Geological Society of America Special Paper 240, 71 p., 8 plates.

Densmore, A. L., and Anderson, R. S., 1994, Recent tectonic geomorphology of Panamint Valley, California: American Geophysical Union, EOS, Fall Meeting Abstracts with Programs, p. 296.

dePolo, C.M., Clark, D.G., Slemmons, D.B., and Ramelli, A.R., 1991, Historical surface faulting in the Basin and Range province, western North America—Implications for fault segmentation: Journal of Structural Geology, v. 13, n. 2, p. 123-136.

Dohrenwend, J.C., Menges, C.M., Schell, B A., and Moring, B.C., 1991, Reconnaissance photogeologic map of young faults in the Las Vegas 1° x 2° quadrangle, Nevada, California, and Arizona: U. S. Geological Survey, Miscellaneous Field Studies Map MF-2182, 1:250,000.

Dohrenwend, J.C., Schell, B.A., McKittrick, M.A., and Moring, B.C., 1992, Reconnaissance photogeologic map of young faults in the Goldfield 1°x2° quadrangle, Nevada and California: U. S. Geological Survey Miscellaneous Field Studies Map MF-2183, 1:250,000.

Doser, D.D., and Smith, R.B., 1985, Source parameters of the October 28, 1983 Borah Peak, Idaho earthquake from body wave analysis: Bulletin of the Seismological Society of America, v. 75, p. 1041-1051.

Doser, D.D., and Smith, R.B., 1989, An assessment of source parameters of earthquakes in the Intermontane region of the United States: Bulletin of the Seismological Society of America, v. 79, p. 1383-1409.

Eddington, P.J., Smith, R.B., and Renggli, C., 1987, Kinematics of Basin-Range intraplate extension, *in* Coward, M.P., Dewey, J.F., and Hancock, P.L., eds., Continental Extension: London Geological Society, Special Publication 28, p. 371-392.

Fauld, J. E., Bell, J. W., Feuerbach, D. L., and Ramelli, A. R. 1994, Geologic map of the Crater Flats area: Nevada Bureau of Mines & Geology Map 101, scale 1:24,000.

Fernald, A.T., Corchary, G.S., Williams, W.P., and Colton, R.B., 1968, Surficial deposits of Yucca Flat area, Nevada Test Site, *in* Eckel, E. B., eds., Nevada Test Site: Geological Society of America, Memoir 110, p. 49-55.

Ferrill, D.A., Stamatakos, J.A., Jones, S.M., Rahe, B., McKague, H.L., Martin, R.H., and Morris, A.P., 1996, Quaternary slip history of the Bare Mountain Fault (Nevada) from the morphology and distribution of alluvial fan deposits: Geology, v.24, n. 6, p.559-562.

Fossen, H., and Gabrielsen, R.H., 1996, Experimental modeling of extensional fault systems by use of plaster: Journal of Structural Geology, v. 18, n. 5, p. 673-687.

Frankel, A., 1995, Mapping seismic hazard in the Central and Eastern United States: Bulletin of the Seismological Society of America, v. 66, p. 8-21.

Frizzell, V.A., Jr., and Shulters, J., 1990, Geologic map of the Nevada Test Site, southern Nevada: U.S. Geological Survey Miscellaneous Investigations Series Map I-2046, 1 plate (1:100,000).

Hancock, P.L., and Barka, A.A., 1987, Kinematic indicators on active normal faults in western Turkey: Journal of Structural Geology, v. 9, n. 5/6, p. 573-584.

Hanks, T.C., and Kanamori, H., 1979, A moment magnitude scale: Journal of Geophysical Research, v. 84, p. 2348-2350.

Hinrichs, E.N., 1968, Geologic map of the Camp Desert Rock quadrangle, Nye County, Nevada: U. S. Geological Survey Geologic Quadrangle Map GQ-726, 1:24,000.

Hoisch, T.D., Heizler, M.T., and Zartman, R.E., 1997, Timing of detachment faulting in the Bullfrog Hills and Bare Mountain area, southwest Nevada: inferences from 40Ar/39Ar, K-Ar, U-Pb and fission-track thermochronology: Journal of Geophysical Research, v. 102, n. B2, p. 2815-2833.

Hudson, M.R., Sawyer, D.A., and Warren, R.G., 1994, Paleomagnetism and rotation constraints for the middle Miocene southwestern Nevada volcanic field: Tectonics, v. 13, n. 2, p. 258-277.

Jackson, J., and White, N., 1989, Normal faulting in the upper continental crust: observations from regions of active extension: Journal of Structural Geology, v. 11, p. 15-36.

Jennings, C. W., 1994, Fault activity map of California and adjacent areas with locations and ages of recent volcanic eruptions: California Division of Mines and Geology, California Geologic Data Map Series, Map No. 6, scale 1:750,000.

Kamamori, H., and Allen, C.R., 1986, Earthquake repeat time and average stress drop, *in* Das, S., Boatwright, J., and Scholz, C.H., eds. Earthquake Source Mechanics: Geophysical Monograph 37, Maurice Ewing v. 6, Washington, D.C., American Geophysical Union.

Lipman, P.W., and McKay, E.J., 1965, Geologic map of the Topopah Spring SW quadrangle, Nye County, Nevada: U. S. Geological Survey Quadrangle Map GQ-439, scale 1:24,000.

Maldonado, F., 1985, Geologic map of the Jackass Flats area, Nye County, Nevada: U.S. Geological Survey, Miscellaneous Investigations, Map I-1519, 1 plate (1:48,000).

Mason, D.B., 1996, Earthquake magnitude potential of the Intermountain seismic belt, USA, from surface-parameter scaling of late Quaternary faults: Bulletin of the Seismological Society of America, v. 86, p. 1487-1506.

McKeown, F.A., Healey, D.L., and Miller, C.H., 1976, Geologic map of the Yucca Lake Quadrangle, Nye County, Nevada: U. S. Geological Survey Geologic Quadrangle Map GQ-1327, scale 1:24,000.

Melosh, H.J., 1990, Mechanical basis for low-angle normal faulting in Basin and Range province: Nature, v. 343, p. 331-335.

Mendoza, C., and Hartzell, S.H., 1988, Inversion for slip distribution using teleseismic P-waveforms: North Palm Springs, Borah Peak, and Michoacan earthquakes: Bulletin of the Seismological Society of America, v. 78, p. 1092-1111.

Meremonte, M., Gomberg, J., and Cranswick, E., 1995, Constraints on the 29 June 1992 Little Skull Mountain, Nevada, earthquake sequence provided by robust hypocenter estimates: Bulletin of the Seismological Society of America, v. 85, n. 4, p. 1039-1049.

Minor, S.A., Sawyer, D.A., Wahl, R.R., Frizzel, V.A., Jr., Schilling, S.P., Warren, R.G., Orkild, P.P., Coe, F.A., Hudson, M.R., Fleck, R.J., Lanphere, M.A., Swadley, WC, and Cole, J.C., 1993, Preliminary geologic map of the Pahute Mesa 30'x60' quadrangle, Nevada: U.S. Geological Survey Open-File Report 93-299, 39 p.

Minor, S. A., Hudson, M. R., and Fridrich, C. J., 1996, Fault-slip data bearing on the tectonic development of northern Crater Flat basin, southern Nevada [abs.]: Geological Society of America Abstracts with Programs, v. 28, n. 7., p. A192.

Monsen, S.A., Carr, M.D., Reheis, M.C., and Orkild, P.P., 1992, Geologic map of Bare Mountain, Nye County, Nevada: U.S. Geological Survey Miscellaneous Investigations Series Map I-2201, 1:24,000 scale.

Morris, A., Ferrill, D. A., and Henderson, D. B., 1996, Slip-tendency analysis and fault reactivation: Geology, v. 24, p. 275-278.

Nicol, A., Walsh, J.J., Watterson, J., and Gillespie, P.A., Fault size distributions-are they really power-law?, , Journal of Structural Geology, v. 18, p. 191-197.

Okaya, D.A., and Thompson, G.A., 1985, Geometry of Cenozoic extensional faulting, Dixie Valley, Nevada: Tectonics, v. 4, n. 1, p. 107-125.

Orkild, P.P., Sargent, K.A., and Snyder, R.P., 1969, Geologic map of Pahute Mesa, Nevada Test Site and vicinity, Nye County: U.S. Geological Survey, Miscellaneous Geologic Investigations Map I-567, 1 plate (1:48,000).

Peterson, F.F., Bell, J.W., Dorn, R.I., Ramelli, A.R., and Ku, T.-L., 1995, Late Quaternary geomorphology and soils in Crater Flat, Yucca Mountain, southern Nevada: Geological Society of America Bulletin, v. 107, n. 4, p. 379-395.

Piety, L. A., 1995, Compilation of known and suspected Quaternary faults within 100 km of Yucca Mountain, Nevada and California: U.S. Geological Survey Open-File Report 94-112, 404 p.

Poole, F.G., Elston, D.P., and Carr, W.J., 1965, Geologic map of the Cane Spring Quadrangle, Nye County, Nevada: U.S. Geological Survey Geologic Map GQ-455, scale 1:24,000.

Reheis, M.C., 1988, Preliminary study of Quaternary faulting on the east side of Bare Mountain, Nye County, Nevada, *in* Carr, M.D., and Yount, J.C., eds., Geologic and hydrologic investigations of a potential nuclear waste disposal site at Yucca Mountain, southern Nevada: U.S. Geological Survey Bulletin 1790, p. 103-111.

Reheis, M.C., 1991, Aerial photographic interpretation of lineaments and faults in late Cenozoic deposits in the eastern parts of the Saline Valley 1:100,000 Quadrangle, Nevada and California, and the Darwin Hills 1:100,000 Quadrangle, California: U.S. Geological Survey Open-File Report 90-500, 6 p., 2 plates.

Reheis, M.C., 1992, Aerial photographic interpretation of lineaments and faults in late Cenozoic deposits in the Cactus Flat and Pahute Mesa 1:100,000 quadrangles and the western parts of the Timpahute Range, Pahranagat Range, Indian Springs, and Las Vegas 1:100,000 Quadrangles, Nevada: U.S. Geological Survey Open-File Report 92-193, 14 p., 3 plates.

Reheis, M.C. and Noller, J.S., 1991, Aerial photographic interpretation of lineaments and faults in late Cenozoic deposits in the eastern part of the Benton Range 1:100,000 Quadrangle and the Goldfield, Last Chance Range, Beatty, and Death Valley Junction 1:100,000 Quadrangles, Nevada and California: U.S. Geological Survey Open-File Report 90-41, 9 p., 4 plates.

Richins, W.D., Smith, R.B., Langer, C.J., Zollweg, J.E., King, J.J., and Pechmann, J.C., 1985, The 1983 Borah Peak, Idaho earthquake: Relationship of aftershocks to the mainshock, surface faulting, and regional tectonics, Workshop XXVIII on "The Borah Peak Earthquake": U.S. Geological Survey Open-File Report, 85-290, p. 285-310.

Rogers, A. M., Corbett, E.J, Priestley, K., and dePolo, D, 1991, The seismicity of Nevada and some adjacent part of the Great Basin, *in* Slemmons, D.B., Engdahl, E.R., Zoback, M.L. and Blackwell, D.D., eds., Neotectonics of North America: Geological Society of America, SMV V-1, Decade Map v. 1, p. 153-184.

Scholz, C. H., 1990, The Mechanics of Earthquakes and Faulting: New York, Cambridge University Press, 439 p.

Scholz, C.H., and Aviles, C.A., 1986, The fractal geometry of faults and faulting, *in* Das, S., Boatwright, J., and Scholz, C.H., eds., Earthquake Source Mechanics: American Geophysical Union Monograph 37, p. 147-155.

Schweickert, R.A., and Lahren, M.M., 1997, Strike-slip fault system in Amargosa Valley and Yucca Mountain, Nevada: Tectonophysics, v. 272, n. 1, p. 25-42.

Schweig, E.S., III, 1989, Basin-Range tectonics in Darwin Plateau, southwestern Great Basin, California: Geological Society of America Bulletin, v. 101, n. 5, p. 652-662.

Scott, R.B., 1990, Tectonic setting of Yucca Mountain, southwest Nevada, *in* Wernicke, B. P., ed., Basin and Range extensional tectonics near the latitude of Las Vegas, Nevada: Boulder, Colorado ,Geological Society of America Memoir 176, p. 251-282.

Scott, R.B., and Bonk, J., 1984, Preliminary geologic map of Yucca Mountain, Nye County, Nevada with geologic sections: U. S. Geological Survey Open File Report 84-494, 9 p., map scale 1:12,000.

Seed, H.B., and Idriss, I.M., 1982, Ground motions and soil liquefactions during earthquakes: Berkeley, California, Earthquake Engineering Research Institute, 134 p.

Shroba, R.R., Muhs, D.R., and Rosholt, J.N., 1988, Uranium-trend and uranium-series age estimates of surficial and fracture-fill deposits on the Carpetbag fault system, Nye County, Nevada: Geologic Society of America, Abstracts with Programs, v. 20, p. 231.

Sibson, R.H., 1982, Fault zone models, heat flow, and the depth distribution of earthquakes in the continental crust of the United States: Bulletin of the Seismological Society of America, v. 72, p. 151-163.

Simonds, F.W., *et al.*, 1995, Map showing fault activity of the Yucca Mountain area, Nye County, Nevada: U.S. Geological Survey Miscellaneous Investigations Series Map I-2520, 30 p., scale 1:24,000.

Slemmons, D.B., 1967, Pliocene and Quaternary crustal movements of the Basin and Range Province, USA: Journal of Geoscience, Osaka City University, v. 10, p. 91-103.

Smith, R.B. and Arabasz, W.J., 1991, Seismicity of the Intermountain Seismic Belt, *in* D.B. Slemmons, E.R. Engdahl, M.L. Zoback and D. D. Blackwell, eds., Neotectonics of North America: Geological Society of America, SMV V-1, Decade Map Volume 1, p. 185-228.

Smith, R.B. and Bruhn, R.L., 1984, Intraplate extensional tectonics of the western U.S. Cordillera: Inferences on structural style from seismic reflection data, regional tectonics and thermal-mechanical models of brittle-ductile deformation: Journal of Geophysical Research, v. 89, p. 5733-5762.

Smith, R.B., Nagy, W.C., Julander, K.A., Viveiros, J.J., Barker, C.A., and Gants, D.G., 1989, Geophysical and tectonic framework of the eastern Basin and Range-Colorado Plateau-Rocky Mountain transition, *in* Pakiser, L.C. and Mooney, W.C., eds., Geophysical Framework of the Continental U.S.: Geological Society of America Memoir 172, p. 205-233.

Smith, R.P., and Jackson, S.M., 1996, Paleoseismology and seismic hazards evaluations in extensional volcanic terrains: Journal of Geophysical Research, v. 10, p. 6,277-6,292.

Snyder, D.B., and Carr, W.J., 1984, Interpretation of gravity data in a complex volcano-tectonic setting, southwestern Nevada: Journal of Geophysical Research, v. 89, n. B12, p. 10,193-10,206.

Stein, R.S., and Barrientos, S.E., 1985, Planar high-angle faulting in the Basin and Range: geodetic analysis of the 1983 Borah Peak, Idaho, earthquake: Journal of Geophysical Research, v. 90, no. B13, p. 11,355-11,366.

Stepp, J. C., 1972, Analysis of completeness of the earthquake sample in the Puget Sound area and its effects on statistical estimates of earthquake hazard: Proceedings, First Microzonation Conference, Seattle, Washington, p. 897-909.

Stewart, J.H., 1988, Tectonics of the Walker Lane Belt, western Great Basin-Mesozoic and Tertiary deformation in a zone of shear, *in* Ernst, W.G., ed., Metamorphism and crustal evolution of the western United States, Rubey Volume VII: Englewood Cliffs, New Jersey, Prentice Hall, p. 683-713.

Stock, J.M., Healy, J.H., Hickman, S.H., and Zoback, M.D., 1985, Hydraulic fracturing stress measurements at Yucca Mountain, Nevada, and relationship to the regional stress field: Journal of Geophysical Research, v. 90, n. B10, p. 8691-8706.

Swadley, W.C., and Hoover, D.L., 1990, Geologic Map of the surficial deposits of the Yucca Flat area, Nye County, Nevada: U.S. Geological Survey, Miscellaneous Investigations Series Map I-2047, 1 plate (1:48,000).

Swadley, W.C., and Huckins, H.E., 1990, Geologic map of the surficial deposits of the Skull Mountain Quadrangle, Nye County, Nevada: U.S. Geological Survey, Miscellaneous Investigation Series, Map I-1972, 1 plate (1:24,000).

Veneziano, D., and Van Dyck, J., 1985, Statistical discrimination of *aftershocks* and their contribution to seismic hazard: Seismic Hazard Methodology for Nuclear Facilities in the Eastern United States: EPRI Res. Project No. P101-29, EPRI/SOG 85-1, v. 2, Appendix A-4.

Wells, D.L., and Coppersmith, K.J., 1994, New empirical relationships among magnitude, rupture length, rupture width, rupture area, and surface displacement: Bulletin of the Seismological Society of America, v. 84, n. 4, p. 974-1002.

Wesnousky, S. G., 1986, Earthquakes, Quaternary faults, and seismic hazard in California: Journal of Geophysical Research, v. 91, p. 12,587-12,631.

Wheeler, R.L., 1989, Persistent segment boundaries on basin-range normal faults, *in* Schwartz, D.P. and Sibson, R.H., eds., Fault segmentation and controls of rupture initiation and termination: U.S. Geological Survey Open File Report 89-315, p.432-444.

Winograd, I.J., and Thordarson, W., 1975, Hydrogeologic and hydrochemical framework, south-central Great Basin, Nevada-California, with special reference to the Nevada Test Site: U. S. Geological Survey Professional Paper 712-C, 126 p.

Wright, L.A., 1989, Overview of the role of strike-slip and normal faulting in the Neogene history of the region northeast of Death Valley, California-Nevada, *in* Ellis, M. A., ed., Late Cenozoic evolution of the southern Great Basin: Nevada Bureau of Mines and Geology Open File Report 89-1, p. 1-11.

Youngs, R.R., and Coppersmith, K.J., 1985, Implications of fault slip rates and earthquake recurrence models for probabilistic seismic hazard estimates: Bulletin of the Seismological Society of America, v. 75, p. 939-964.

Youngs, R.R., Swan, F.H., III, Power, M.S., Schwartz, D.P., and Green, R.K., 1987, Probabilistic analysis of earthquake and ground shaking hazard along the Wasatch Front, Utah, *in* Gori, P.O., and Hays, W.W., eds., Assessment of Regional Earthquake Hazards and Risk Along the Wasatch Front, Utah: U.S. Geological Survey Open File Report 87-585, p. M-1 to M-100.

Yount, J.C., Shroba, R.R., McMasters, C.R., Huckins, H.E., and Rodriguez, E. A., 1987, Trench logs from a strand of the Rock Valley fault system, Nevada Test Site, Nye County, Nevada: U.S. Geological Survey, Miscellaneous Field Studies Map MF-1824, 1 plate.

Zhang, P., Ellis, M., Slemmons D. B., and Moa, F., 1990, Right-lateral displacements and the Holocene slip rate associated with prehistoric earthquakes along the southern Panamint Valley fault zone: Implications for southern basin and range tectonics and coastal California deformation: Journal of Geophysical Research, v. 95, p. 4857-4872.

## TABLE SDO-1
## MAXIMUM MAGNITUDES FOR SOURCE ZONES

| Zone | Maximum Magnitude [1] | Name of Zone and Comments |
|---|---|---|
| 1 | | **Goldfield-Spring Mountain Zone including Yucca Mountain site:** |
| | 6.4 ± 0.2 MBE | a) within 100 km of the site |
| | | b) outside 100 km |
| | Ms 7.1 ± 0.2 | South, Frenchman Mtns. Fault |
| | Ms 7.0 ± 0.2 | North, Emigrant Peak fault |
| 2 | | **Death Valley Zone** |
| | 6.4 ± 0.2 MBE | a) within 100 km |
| | | b) outside 100 km |
| | Ms 7.4 ± 0.2 | White Mountain fault system |
| 3 | | **Basin-Range Zone** |
| | 6.4 ± 0.2 MBE | a) within 100 km |
| | | b) outside 100 km |
| | Ms 7.4 ± 0.2 | Railroad Valley fault system |

[1] Ms should be equivalent to Mw (Hanks and Kanamori, 1979).

## TABLE SDO-2
## MAGNITUDE SCALING RELATIONSHIPS USED

| | |
|---|---|
| **Magnitude versus Length** | |
| Mason (1996) | |
| Mw = 5.08 + 1.16 log L | extensional environments; all displacement types |
| Wells and Coppersmith (1994) | |
| Mw = 4.86 + 1.32 log L | All environments (excl. subduction zones) |
| Mw = 5.16 + 1.12 log L | normal-slip faults |
| Mw = 5.08 + 1.16 log L | strike-slip faults |
| | all displacement types |
| **Magnitude versus Maximum Surface Displacement** | |
| Mason (1996) | |
| Ms = 6.81 + 0.74 log D | extensional environments; all types |
| Wells and Coppersmith (1994) | |
| Mw = 6.61 + 0.71 log D | All environments (excl. subduction zones) |
| Mw = 6.81 + 0.78 log D | normal-slip faults |
| Mw = 6.69 + 0.74 log D | strike-slip faults |
| | all displacement types |
| **Magnitude versus Fault Area** | |
| Wells and Coppersmith (1994) | |
| Mw = 3.93 + 1.02 log A | all environments (excl. subduction zones) |
| Mw = 3.98 + 1.02 log A | normal-slip faults |
| Mw = 4.07 + 0.98 log A | strike-slip faults |
| | all displacement types |
| **Magnitude versus Length x Displacement** | |
| Mason (1996) | |
| Ms = 5.95 + 0.55 log LD | extensional environments; all displacement types |
| **Magnitude versus Length and Slip Rate** | |
| Anderson *et al.* (1996) | |
| Mw = 5.12 + 1.16 log L - 0.20 log SR | 15-20 km maximum seismogenic depth |
| | all displacement types |
| **Magnitude via Seismic Moment** | |
| Hanks and Kanamori (1979) | all environments |
| Mw = 2/3 log Mo - 10.7 | all displacement types |
| **Average Displacement versus surface length** | |
| Wells and Coppersmith (1994) | |
| log (AD) = -0.99 + 1.24 log L | all environments (excl. subduction zones) normal-slip faults |
| log (AD) = -0.70 + 1.04 log L | strike-slip faults |
| log (AD) = -1.43 + 0.88 log L | all faults |

# TABLE SDO-3
# PARAMETERS FOR REGIONAL FAULT SOURCES
## (Page 1 of 2)

| Fault (map designation) | | Sense of Displacement | Length | | | Maximum Surface Displacement Per Event | | | Slip Rate | | | Quaternary Activity Relative Weighting | |
|---|---|---|---|---|---|---|---|---|---|---|---|---|---|
| | | | Minimum | Preferred | Maximum | Minimum | Preferred | Maximum | Minimum | Preferred | Maximum | Yes | No |
| Amaragosa River | (AR) | rl | 17 | 17 | 28 | | | | 0.001 | 0.01 | 0.05 | 1 | 0 |
| Ash Hill | (AH) | rl | 33 | 55 | 90 | | | | 0.21 | 0.3 | 0.38 | 1 | 0 |
| Bare Mountain | (BM) | n | 18 | 23 | 30 | 1.2 | 1.5 | 1.8 | 0.006 | 0.01 | 0.2 | 1 | 0 |
| Belted Range | (BLR) | n | 22 | 34 | 46 | | | | 0.01 | 0.05 | 0.1 | 1 | 0 |
| Buried Hills | (BH) | n | 15 | 18 | 25 | | | | 0.001 | 0.01 | 0.05 | 1 | 0 |
| Buried Strike-slip | (T6-SS) | rl | 20 | 27 | 120 | | | | 0.001 | 0.005 | 0.02 | 0.4 | 0.6 |
| Cane Spring | (CS) | ll | 19 | 26 | 30 | | | | 0.005 | 0.01 | 0.05 | 0.8 | 0.2 |
| Carpetbag | (CB) | n | 17 | 28 | 39 | | | | 0.001 | 0.005 | 0.01 | 0.8 | 0.2 |
| Carrara (Highway 95) | (H95) | rl | 11 | 26 | 41 | | | | 0.0005 | 0.001 | 0.005 | 0.2 | 0.8 |
| Central Death Valley | (DV) | rn | 41 | 61 | 75 | 2.5 | 3.5 | 4.5 | 2.6 | 3.8 | 7.4 | 1 | 0 |
| E. Pintwater Range | (EPR) | n | 28 | 36 | 58 | | | | 0.001 | 0.005 | 0.01 | 1 | 0 |
| Eleana Range | (ER) | n | 11 | 15 | 15 | | | | 0.003 | 0.01 | 0.05 | 1 | 0 |
| Furnace Creek | (FC) | rl | 85 | 105 | 195 | 5.5 | 6 | 6.5 | 4 | 8 | 10 | 1 | 0 |
| Grapevine Mountains | (GM) | n | 26 | 26 | 32 | | | | 0.003 | 0.01 | 0.05 | 1 | 0 |
| Hunter Mountain | (HM) | nrl | 46 | 64 | 65 | | | | 1.3 | 2 | 2.7 | 1 | 0 |
| Jackass Flats "Gravity" | (JFG) | n | 26 | 34 | 44 | | | | 0.0005 | 0.005 | 0.05 | 0.9 | 0.1 |
| Kawich Range | (KR) | n | 22 | 32 | 45 | | | | 0.001 | 0.005 | 0.01 | 1 | 0 |
| Keane Wonder | (KW) | n | 19 | 27 | 29 | | | | 0.001 | 0.005 | 0.05 | 0.8 | 0.2 |
| Mine Mountain | (MM) | ll | 21 | 21 | 35 | | | | 0.005 | 0.01 | 0.09 | 1 | 0 |
| N. Emigrant Valley | (EVN) | rl? | 18 | 37 | 45 | | | | 0.01 | 0.02 | 0.08 | 1 | 0 |
| Oak Spring Butte | (OAK) | n | 9 | 16 | 19 | | | | 0.001 | 0.005 | 0.01 | 0.8 | 0.2 |
| Oasis Valley | (OSV) | n | 5 | 8 | 19 | | | | 0.0005 | 0.001 | 0.003 | 0.8 | 0.2 |
| Pahrump Valley | (PRP) | rl | 24 | 61 | 66 | | | | 0.005 | 0.01 | 0.1 | 1 | 0 |
| Pahute Mesa #1 | (PMI) | n | 11 | 13 | 15 | | | | 0.001 | 0.005 | 0.01 | 0.8 | 0.2 |
| Panamint Valley | (PAN) | rl | 82 | 90 | 105 | | | | 1.6 | 2.4 | 3.2 | 1 | 0 |
| Peace Camp | (PC) | nl | 12 | 12 | 30 | | | | 0.005 | 0.01 | 0.09 | 1 | 0 |
| Rock Valley | (RV) | ll | 33 | 48 | 68 | 1.1 | 3.6 | 4.5 | 0.01 | 0.02 | 0.08 | 1 | 0 |

# TABLE SDO-3
## (Page 2 of 2)

| Fault (map designation) | Sense of Displacement | Length | | | Maximum Surface Displacement Per Event | | | Slip Rate | | | Quaternary Activity Relative Weighting | |
|---|---|---|---|---|---|---|---|---|---|---|---|---|
| | | Minimum | Preferred | Maximum | Minimum | Preferred | Maximum | Minimum | Preferred | Maximum | Yes | No |
| South Silent Canyon (SSC) | n | 11 | 14 | 17 | | | | 0.001 | 0.005 | 0.01 | 0.8 | 0.2 |
| Spotted Range (SPR) | n | 17 | 30 | 30 | | | | 0.001 | 0.01 | 0.05 | 1 | 0 |
| Towne Pass (TP) | n | 33 | 38 | 50 | | | | 0.005 | 0.03 | 0.1 | 1 | 0 |
| Wahmonie (WAH) | II | 9 | 15 | 15 | | | | 0.005 | 0.01 | 0.05 | 0.8 | 0.2 |
| West Specter Range (WSR) | n | 10 | 19 | 25 | | | | 0.001 | 0.004 | 0.01 | 1 | 0 |
| West Spring Mountains(WSM) | n | 31 | 36 | 58 | | | | 0.02 | 0.09 | 0.2 | 1 | 0 |
| Western Pintwater Range (WPR) | n | 33 | 54 | 76 | | | | 0.005 | 0.008 | 0.05 | 1 | 0 |
| Yucca Lake (YCL) | n | 12 | 19 | 23 | | | | 0.001 | 0.005 | 0.01 | 0.5 | 0.5 |
| Yucca-Butte (YB) | n | 26 | 34 | 49 | | | | 0.015 | 0.026 | 0.053 | 1 | 0 |

# TABLE SDO-4
# PARAMETERS FOR LOCAL FAULT SOURCES

| FAULT | TOTAL LENGTH | WEIGHTING | FAULT DIP | DOWNDIP WIDTH | WEIGHTING | MAXIMUM SURFACE DISPLACEMENT | WEIGHTING | SLIP RATE | WEIGHTING | MOMENT RATE | EVENT MOMENT | MOMENT MAGNITUDE |
|---|---|---|---|---|---|---|---|---|---|---|---|---|
| | Km | | degrees | km | | (m) | | m/kyr | | dyne-cm/yr | dyne-cm | |
| Solitario Canyon fault | 16 | 0.3 | 55 | 11.1 | 0.2 | 0.7 | 0.3 | 0.009 | 0.3 | 4.436e+20 | 1.72494e+25 | 6.2 |
| (SC) | 18.5 | 0.4 | 55 | 13.3 | 0.4 | 1.2 | 0.4 | 0.015 | 0.4 | 1.107e+21 | 4.42890e+25 | 6.6 |
| | 21.5 | 0.3 | 55 | 17.6 | 0.4 | 1.5 | 0.3 | 0.022 | 0.3 | 2.497e+21 | 8.51400e+25 | 6.9 |
| Iron Ridge fault | 8.3 | 0.3 | 55 | 11.5 | 0.2 | 0.5 | 0.3 | 0.0023 | 0.3 | 6.586e+19 | 7.15875e+24 | 5.9 |
| (IR) | 8.3 | 0.4 | 55 | 14.5 | 0.6 | 0.7 | 0.4 | 0.0033 | 0.4 | 1.191e+20 | 1.26368e+25 | 6.1 |
| | 9 | 0.3 | 55 | 19 | 0.2 | 1 | 0.3 | 0.0051 | 0.3 | 2.907e+20 | 2.85000e+25 | 6.4 |
| Fatigue Wash fault | 16 | 0.3 | 55 | 9.7 | 0.2 | 1 | 0.3 | 0.003 | 0.3 | 1.048e+20 | 1.74600e+25 | 6.2 |
| (FW)) | 17 | 0.4 | 55 | 11.6 | 0.6 | 1.25 | 0.4 | 0.005 | 0.4 | 3.132e+20 | 3.91500e+25 | 6.6 |
| | 20 | 0.3 | 75 | 17.6 | 0.2 | 1.5 | 0.3 | 0.009 | 0.3 | 1.045e+21 | 8.71200e+25 | 6.9 |
| Southern Windy Wash fault | 9 | 0.3 | 45 | 8.5 | 0.2 | 0.6 | 0.3 | 0.009 | 0.3 | 2.066e+20 | 6.88500e+24 | 5.9 |
| (SWW) | 11.5 | 0.4 | 55 | 10.5 | 0.6 | 0.88 | 0.4 | 0.011 | 0.4 | 3.985e+20 | 1.59390e+25 | 6.2 |
| | 15 | 0.3 | 75 | 17.6 | 0.2 | 1 | 0.3 | 0.017 | 0.3 | 1.122e+21 | 3.30000e+25 | 6.5 |
| Paintbrush Canyon fault | 12 | 0.3 | 55 | 14.5 | 0.3 | 0.4 | 0.3 | 0.007 | 0.3 | 3.654e+20 | 1.04400e+25 | 6.0 |
| (PC(N) + PC(S)) | 17.5 | 0.4 | 55 | 17.3 | 0.6 | 1.7 | 0.4 | 0.008 | 0.4 | 7.266e+20 | 7.72013e+25 | 6.8 |
| | 26.2 | 0.3 | 55 | 23 | 0.1 | 2.6 | 0.3 | 0.011 | 0.3 | 1.989e+21 | 2.35014e+26 | 7.3 |
| Paintbrush Canyon (North) | 7 | 0.3 | 55 | 14.5 | 0.3 | 0.4 | 0.3 | 0.007 | 0.3 | 2.132e+20 | 6.09000e+24 | 5.8 |
| (PC(N)) | 12.3 | 0.4 | 55 | 17.3 | 0.6 | 1 | 0.4 | 0.008 | 0.4 | 5.107e+20 | 3.19185e+25 | 6.5 |
| | 18.7 | 0.3 | 55 | 23 | 0.1 | 1.45 | 0.3 | 0.011 | 0.3 | 1.419e+21 | 9.35468e+25 | 6.9 |
| Paintbrush Canyon (South) | 9 | 0.3 | 55 | 14.5 | 0.3 | 0.3 | 0.3 | 0.007 | 0.3 | 2.436e+20 | 5.22000e+24 | 5.8 |
| (PC(S) | 11 | 0.4 | 55 | 17.3 | 0.6 | 1.7 | 0.4 | 0.008 | 0.4 | 4.567e+20 | 4.85265e+25 | 6.6 |
| | 11 | 0.3 | 55 | 23 | 0.1 | 2.6 | 0.3 | 0.011 | 0.3 | 8.349e+20 | 9.86700e+25 | 6.9 |
| Stagecoach Road fault | 4.5 | 0.3 | 55 | 11.5 | 0.2 | 0.6 | 0.3 | 0.0057 | 0.3 | 8.849e+19 | 4.65750e+24 | 5.7 |
| (SCR) | 10 | 0.4 | 55 | 14.5 | 0.6 | 0.8 | 0.4 | 0.017 | 0.4 | 6.656e+20 | 1.56600e+25 | 6.2 |
| | 12 | 0.3 | 55 | 19 | 0.2 | 1.2 | 0.3 | 0.028 | 0.3 | 1.756e+21 | 376200e+25 | 6.5 |

## TABLE SDO-5
## MULTIPLE-FAULT EVENT SCENARIOS AND EVENT MOMENTS FOR LOCAL FAULTS
## (Page 1 of 2)

| FAULT[1] | TOTAL LENGTH | WEIGHTING | FAULT DIP | DOWNDIP WIDTH | WEIGHTING | MAXIMUM SURFACE DISPLACEMENT | WEIGHTING | EVENT MOMENT | MOMENT MAGNITUDE |
|---|---|---|---|---|---|---|---|---|---|
| | km | | degrees | km | | (cm) | | dyne-cm | |
| PC(N) + BR | 8 | 0.3 | 55 | 14.5 | 0.3 | 33 | 0.3 | 5.742e+24 | 5.8 |
| | 14 | 0.4 | 55 | 17.3 | 0.6 | 52 | 0.4 | 1.889e+25 | 6.3 |
| | 19.7 | 0.3 | 55 | 23.2 | 0.1 | 94 | 0.3 | 6.444e+25 | 6.8 |
| PC(N) + PC(S) + BR + SCR | 18.6 | 0.3 | 55 | 14.5 | 0.3 | 33 | 0.3 | 1.335e+25 | 6.1 |
| | 28.8 | 0.4 | 55 | 17.3 | 0.6 | 53 | 0.4 | 3.961e+25 | 6.6 |
| | 34.4 | 0.3 | 55 | 23.2 | 0.1 | 185 | 0.3 | 2.215e+26 | 7.2 |
| PC(N) + PC(S) + BR | 12 | 0.3 | 55 | 14.5 | 0.3 | 33 | 0.3 | 8.613e+24 | 6.0 |
| | 17.5 | 0.4 | 55 | 17.3 | 0.6 | 53 | 0.4 | 2.407e+25 | 6.4 |
| | 26.2 | 0.3 | 55 | 23.2 | 0.1 | 185 | 0.3 | 1.687e+26 | 7.1 |
| SC + SWW | 22 | 0.3 | 55 | 11.1 | 0.2 | 20 | 0.3 | 7.326e+24 | 5.9 |
| | 24.8 | 0.4 | 55 | 13.3 | 0.4 | 35 | 0.4 | 1.732e+25 | 6.2 |
| | 25 | 0.3 | 55 | 17.6 | 0.4 | 50 | 0.3 | 3.300e+25 | 6.5 |
| FW + SWW + SCF | 18.8 | 0.3 | 55 | 9.7 | 0.2 | 47 | 0.3 | 1.286e+25 | 6.1 |
| | 26 | 0.4 | 55 | 11.6 | 0.6 | 105 | 0.4 | 4.641e+25 | 6.6 |
| | 31 | 0.3 | 75 | 17.6 | 0.2 | 165 | 0.3 | 1.333e+26 | 7.0 |
| SWW + SCF | 9 | 0.3 | 45 | 8.5 | 0.2 | 55 | 0.3 | 6.311e+24 | 5.8 |
| | 12.3 | 0.4 | 55 | 10.5 | 0.6 | 62 | 0.4 | 1.201e+25 | 6.1 |
| | 14.4 | 0.3 | 75 | 17.6 | 0.2 | 84 | 0.3 | 3.193e+25 | 6.5 |
| SWW + SCF + NCF | 19.8 | 0.3 | 45 | 8.5 | 0.2 | 7.5 | 0.3 | 1.893e+24 | 5.4 |
| | 22.2 | 0.4 | 55 | 10.5 | 0.6 | 12 | 0.4 | 4.196e+24 | 5.7 |
| | 23 | 0.3 | 75 | 17.6 | 0.2 | 20 | 0.3 | 1.214e+25 | 6.1 |
| ash event | 18.6 | 0.3 | 55 | 14.5 | 0.3 | 115 | 0.3 | 4.652e+25 | 6.6 |
| | 28.8 | 0.4 | 55 | 17.3 | 0.6 | 145 | 0.4 | 1.084e+26 | 7.0 |
| | 34.4 | 0.3 | 55 | 23.2 | 0.1 | 175 | 0.3 | 2.095e+26 | 7.2 |
| PC(N) +PC(S) + SCR | 18.6 | 0.3 | 55 | 14.5 | 0.3 | 26 | 0.3 | 1.052e+25 | 6.0 |
| | 28.8 | 0.4 | 55 | 17.3 | 0.6 | 40 | 0.4 | 2.989e+25 | 6.5 |
| | 34.4 | 0.3 | 55 | 23.2 | 0.1 | 140 | 0.3 | 1.676e+26 | 7.1 |

[1] Fault names are given in Table SDO-4

## TABLE SDO-5
## (Page 2 of 2)

| FAULT[1] | TOTAL LENGTH | WEIGHTING | FAULT DIP | DOWNDIP WIDTH | WEIGHTING | MAXIMUM SURFACE DISPLACEMENT | WEIGHTING | EVENT MOMENT | MOMENT MAGNITUDE |
|---|---|---|---|---|---|---|---|---|---|
| | km | | degrees | km | | (cm) | | dyne-cm | |
| PC(S) + SCR | 15.2 | 0.3 | 55 | 14.5 | 0.3 | 25 | 0.3 | 8.265e+24 | 5.9 |
| | 19.8 | 0.4 | 55 | 17.3 | 0.6 | 57 | 0.4 | 2.929e+25 | 6.4 |
| | 19.8 | 0.3 | 55 | 23.2 | 0.1 | 84 | 0.3 | 5.788e+25 | 6.7 |
| PC(S) + BR | 11 | 0.3 | 55 | 14.5 | 0.3 | 88 | 0.3 | 2.450e+25 | 6.4 |
| | 12.8 | 0.4 | 55 | 17.3 | 0.6 | 167 | 0.4 | 4.767e+25 | 6.6 |
| | 15.6 | 0.3 | 55 | 23.2 | 0.1 | 205 | 0.3 | 1.113e+26 | 7.0 |
| SCR + SC | 20.4 | 0.3 | 55 | 11.1 | 0.2 | 28 | 0.3 | 9.510e+24 | 6.0 |
| | 25.6 | 0.4 | 55 | 13.3 | 0.6 | 59 | 0.4 | 3.013e+25 | 6.5 |
| | 25.6 | 0.3 | 55 | 17.6 | 0.2 | 77 | 0.3 | 5.204e+25 | 6.7 |
| IR + AW | 9.7 | 0.3 | 55 | 11.1 | 0.2 | 50 | 0.3 | 8.075e+24 | 5.9 |
| | 9.7 | 0.4 | 55 | 13.3 | 0.6 | 70 | 0.4 | 1.355e+25 | 6.1 |
| | 11 | 0.3 | 55 | 17.6 | 0.2 | 100 | 0.3 | 2.904e+25 | 6.4 |
| IR + AW + GD | 13.2 | 0.3 | 55 | 11.1 | 0.2 | 50 | 0.3 | 1.099e+25 | 6.1 |
| | 13.2 | 0.4 | 55 | 13.3 | 0.6 | 70 | 0.4 | 1.843e+25 | 6.3 |
| | 13.7 | 0.3 | 55 | 17.6 | 0.2 | 100 | 0.3 | 3.643e+25 | 6.5 |
| FW + SWW | 18.8 | 0.3 | 55 | 9.7 | 0.2 | 30 | 0.3 | 8.206e+24 | 5.9 |
| | 26 | 0.4 | 55 | 11.6 | 0.6 | 105 | 0.4 | 4.604e+25 | 6.6 |
| | 31 | 0.3 | 75 | 17.6 | 0.2 | 165 | 0.3 | 1.307e+26 | 7.0 |
| SWW + FW + NWW | 22.8 | 0.3 | 55 | 9.7 | 0.2 | 14 | 0.3 | 4.644e+24 | 5.7 |
| | 26 | 0.4 | 55 | 11.6 | 0.6 | 20 | 0.4 | 9.048e+24 | 6.0 |
| | 27.4 | 0.3 | 75 | 17.6 | 0.2 | 24 | 0.3 | 1.736e+25 | 6.2 |
| SWW + CWW | 12.6 | 0.3 | 55 | 8.5 | 0.2 | 38 | 0.3 | 6.105e+24 | 5.8 |
| | 15.4 | 0.4 | 55 | 10.5 | 0.6 | 73 | 0.4 | 1.771e+25 | 6.2 |
| | 18 | 0.3 | 75 | 17.6 | 0.2 | 83 | 0.3 | 3.944e+25 | 6.6 |

[1] Fault names are given in Table SDO-4

**Table SDO-6**
**Regressions Used for Estimating Displacement**
Note that the regressions assumed *AD* and *MD* as the independent variable.

| **Regression** | **Reference** |
|---|---|
| $\log AD = 0.63\ \mathbf{M} - 4.45$ | Wells and Coppersmith (1994) |
| $\log AD = 1.24 \log L - 1.99$ | Wells and Coppersmith (1994) |
| $\log AD = \log L - 1.43$ | AAR Team (SSC workshop #4, Jan. 8, 1997) |
| $\log MD = 0.89\ \mathbf{M} - 5.90$ | Wells and Coppersmith (1994) |
| $\log MD = 1.51 \log L - 1.98$ | Wells and Coppersmith (1994) |

where *AD* = average surface displacement in meters; *MD* = maximum surface displacement in meters; **M** = moment magnitude; and *L* = surface rupture length in kilometers.

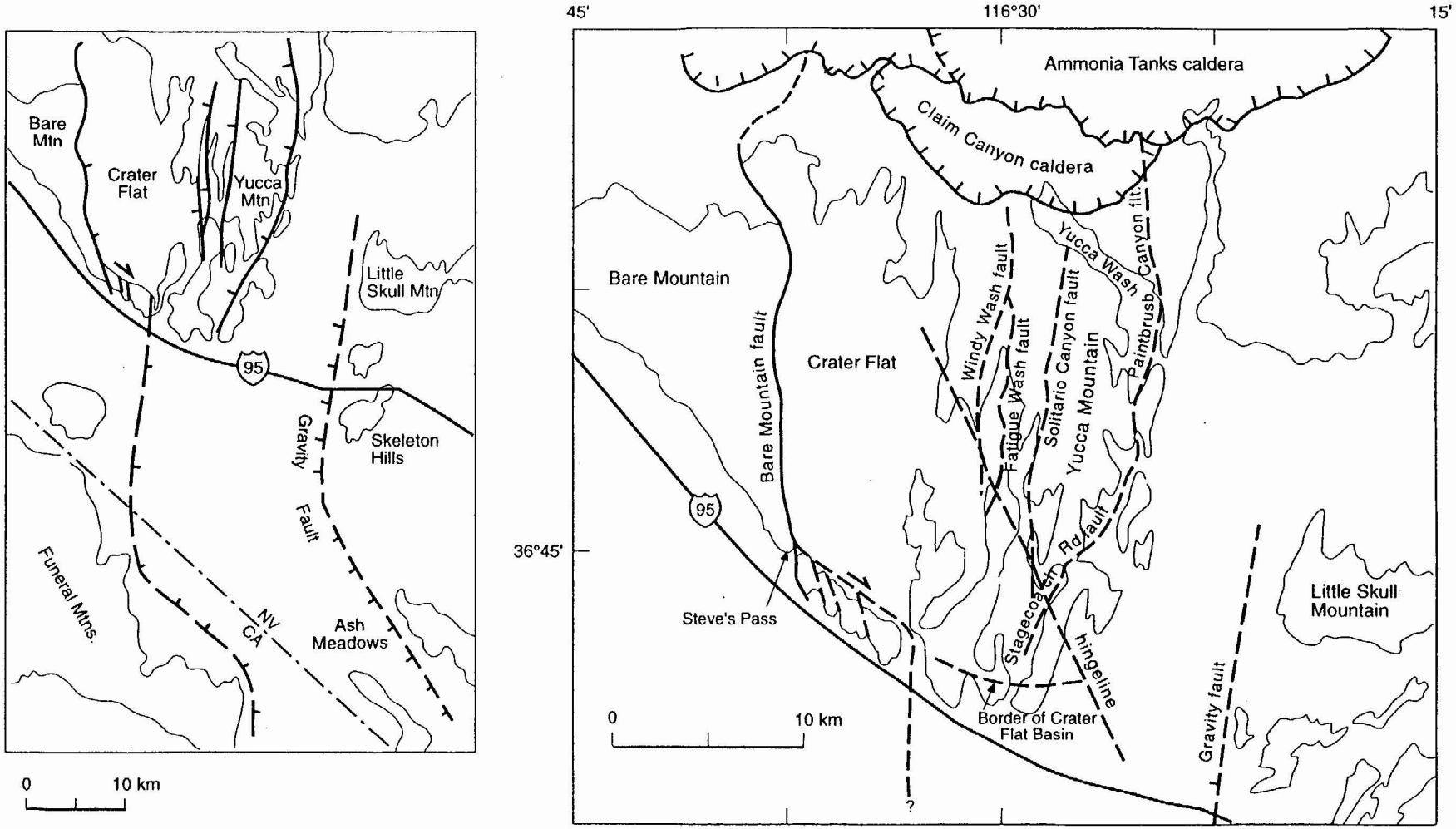


**Figure SDO-1** Map showing location and features of Yucca Mountain and Crater Flat

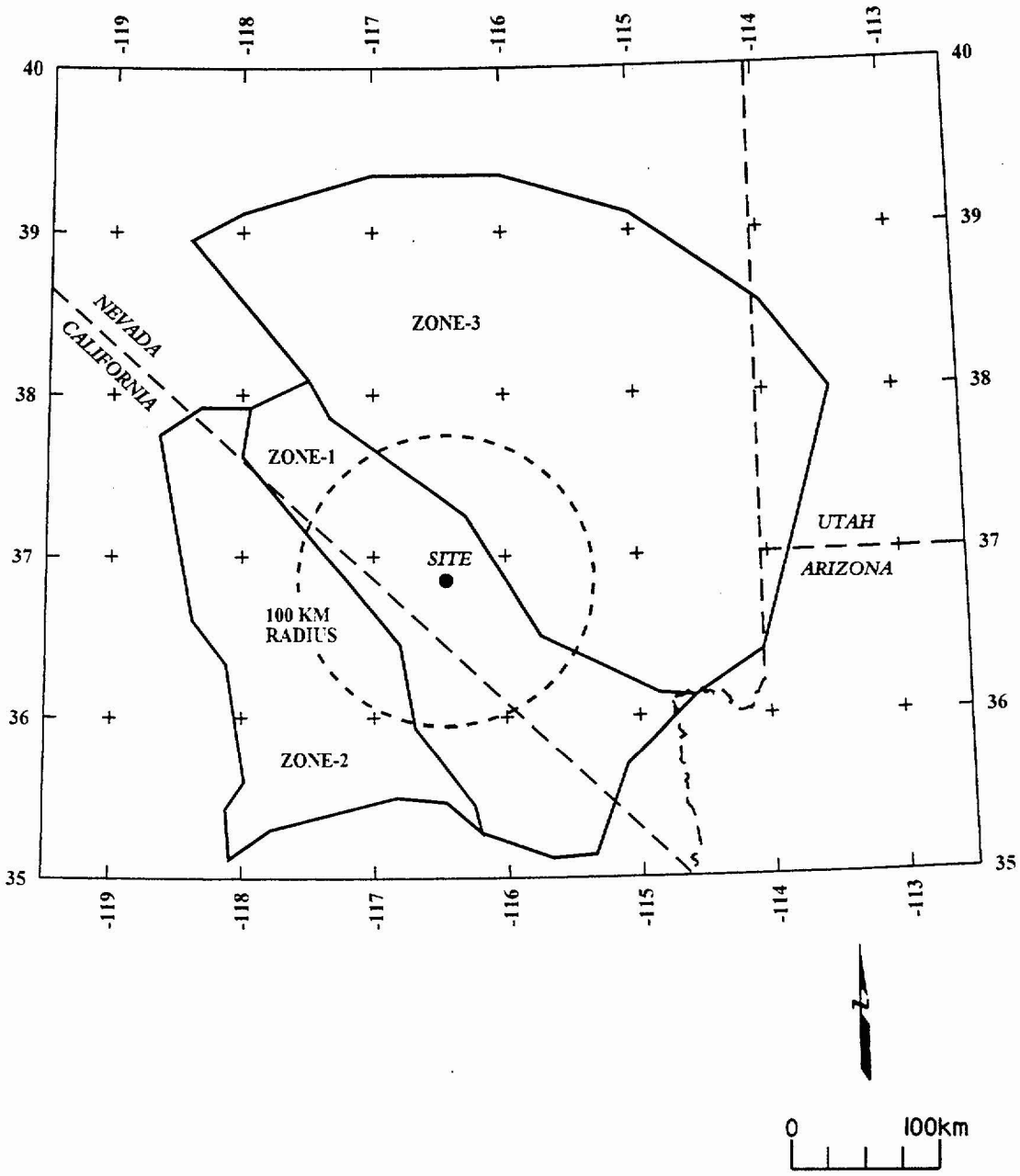


Figure SDO-2 Map showing the boundaries of zones used in the seismic source model

h:\prj\yucca_mt\dgn\1097\plate_t6_reg_zone.dgn 07-NOV-1997 10:16

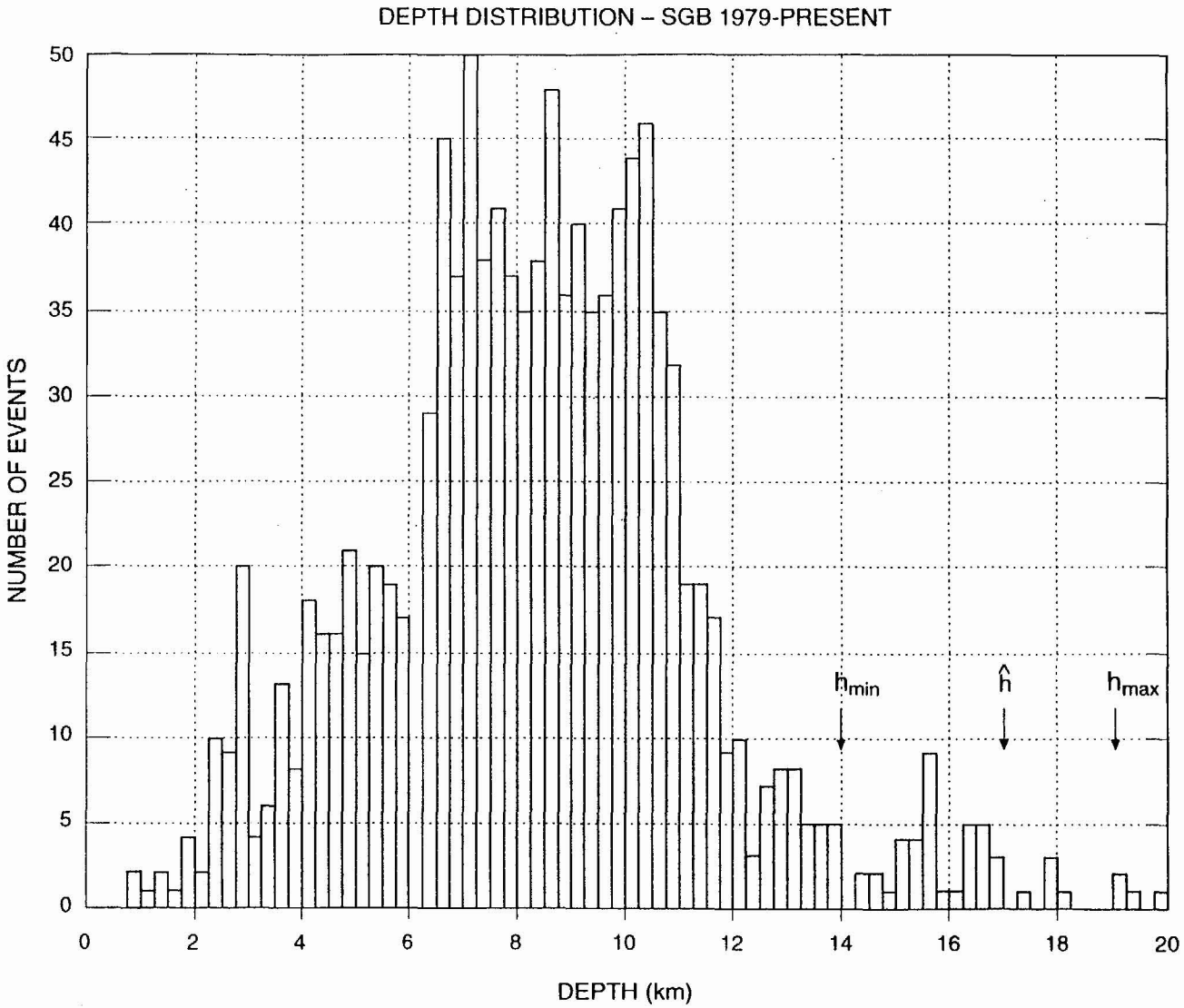


**Figure SDO-3** Depth distribution of hypocenters (focal depth distribution) of earthquakes in the southern Great Basin (SGB)

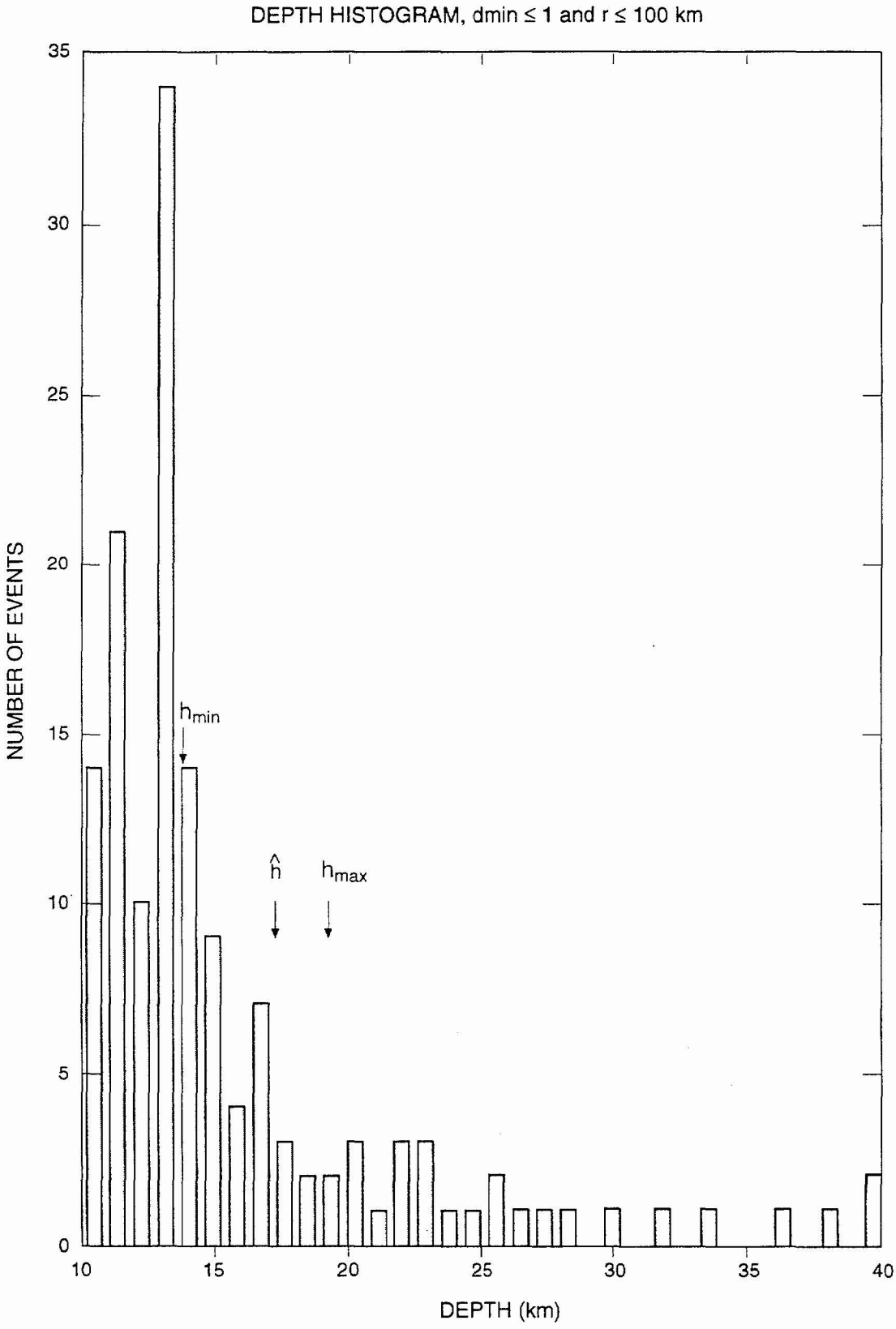


Figure SDO-4 Focal depth distribution of deep earthquakes in the area within r<100 km of Yucca Mountain

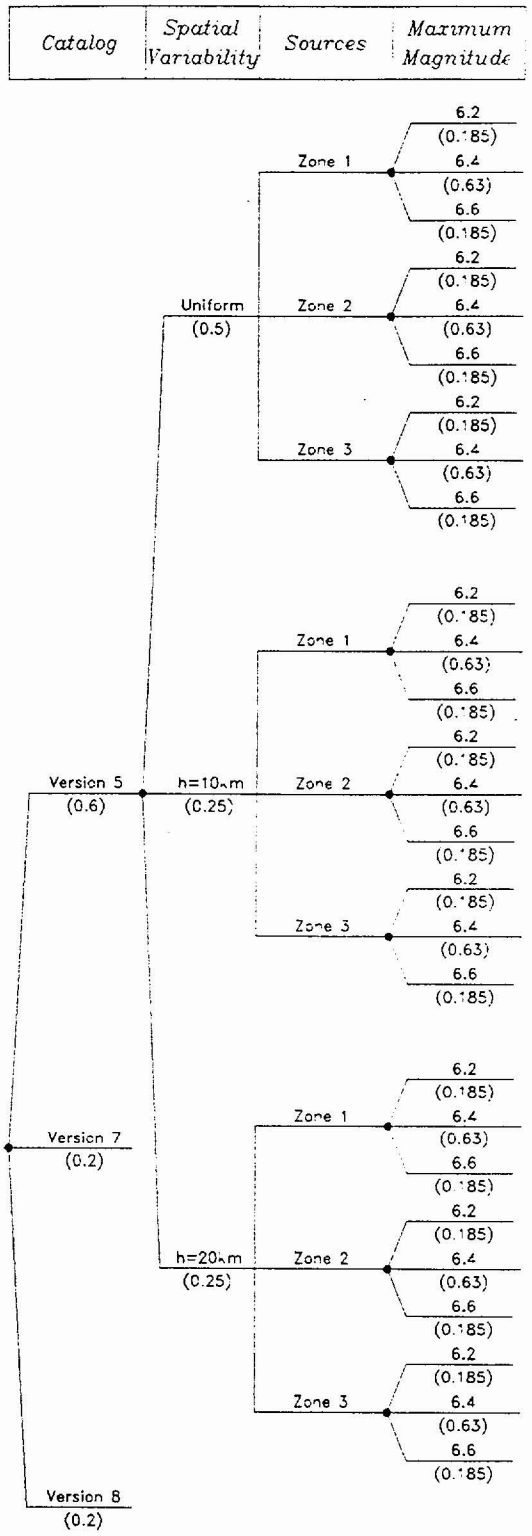


Figure SDO-5 Logic tree for regional source zones

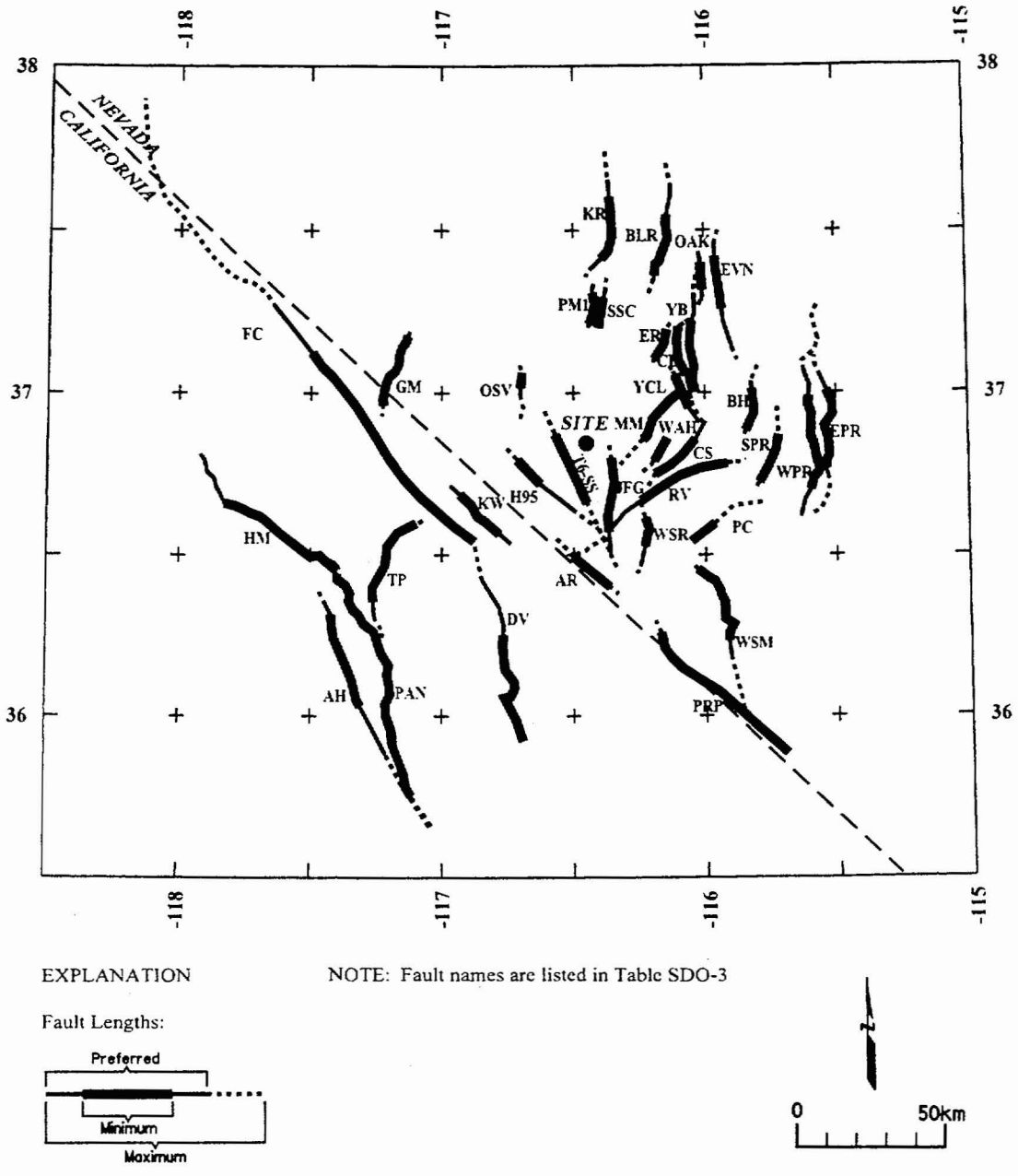


Figure SDO- 6 Map showing regional faults included in the seismic source model.

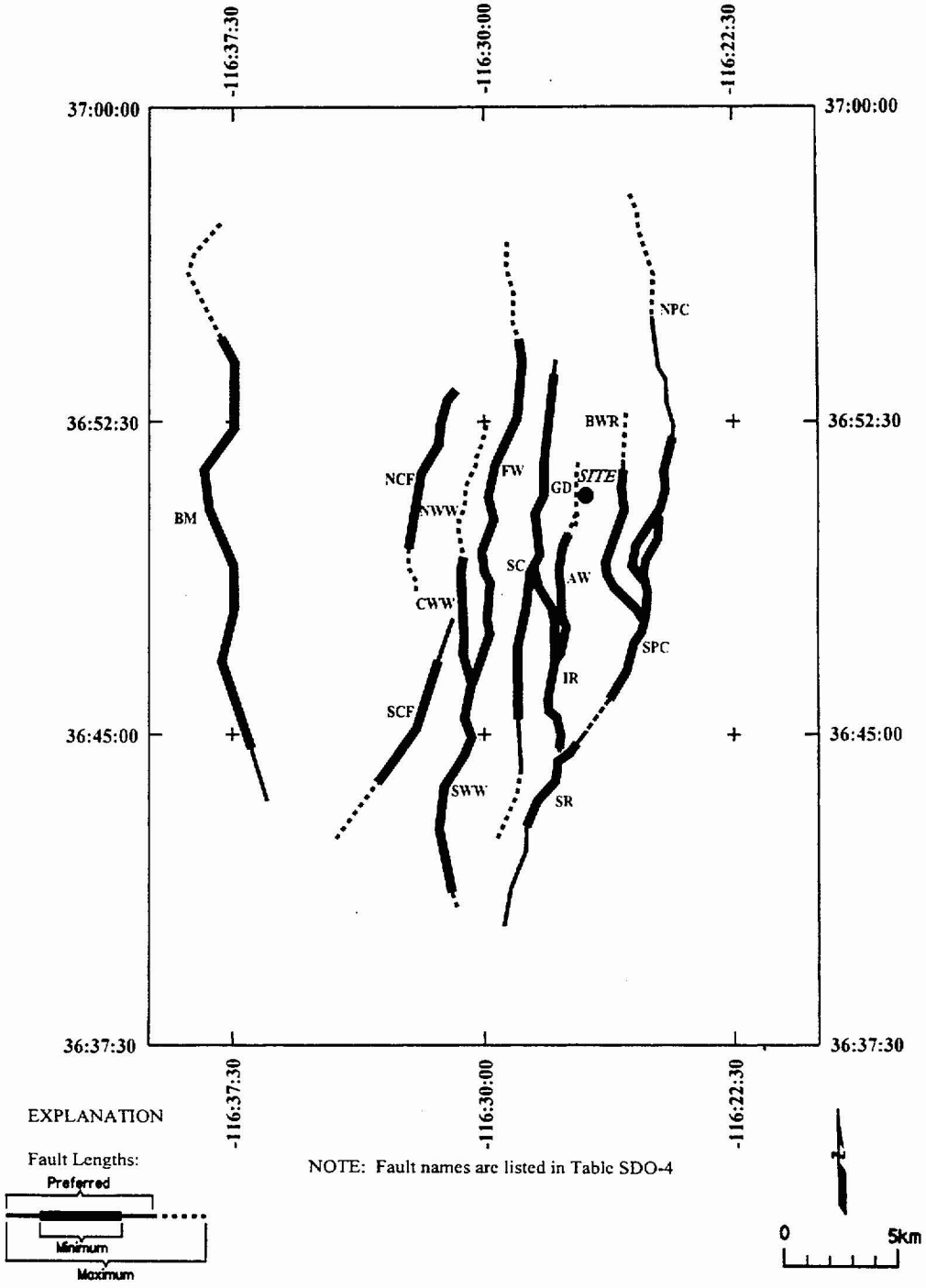


Figure SDO- 7a Map showing local fault sources included in the independent seismic source model

h:\prj\yucca_mt\dgn\1097\plate_t6_jcl_fault.dgn 07-NOV-1997 10:43

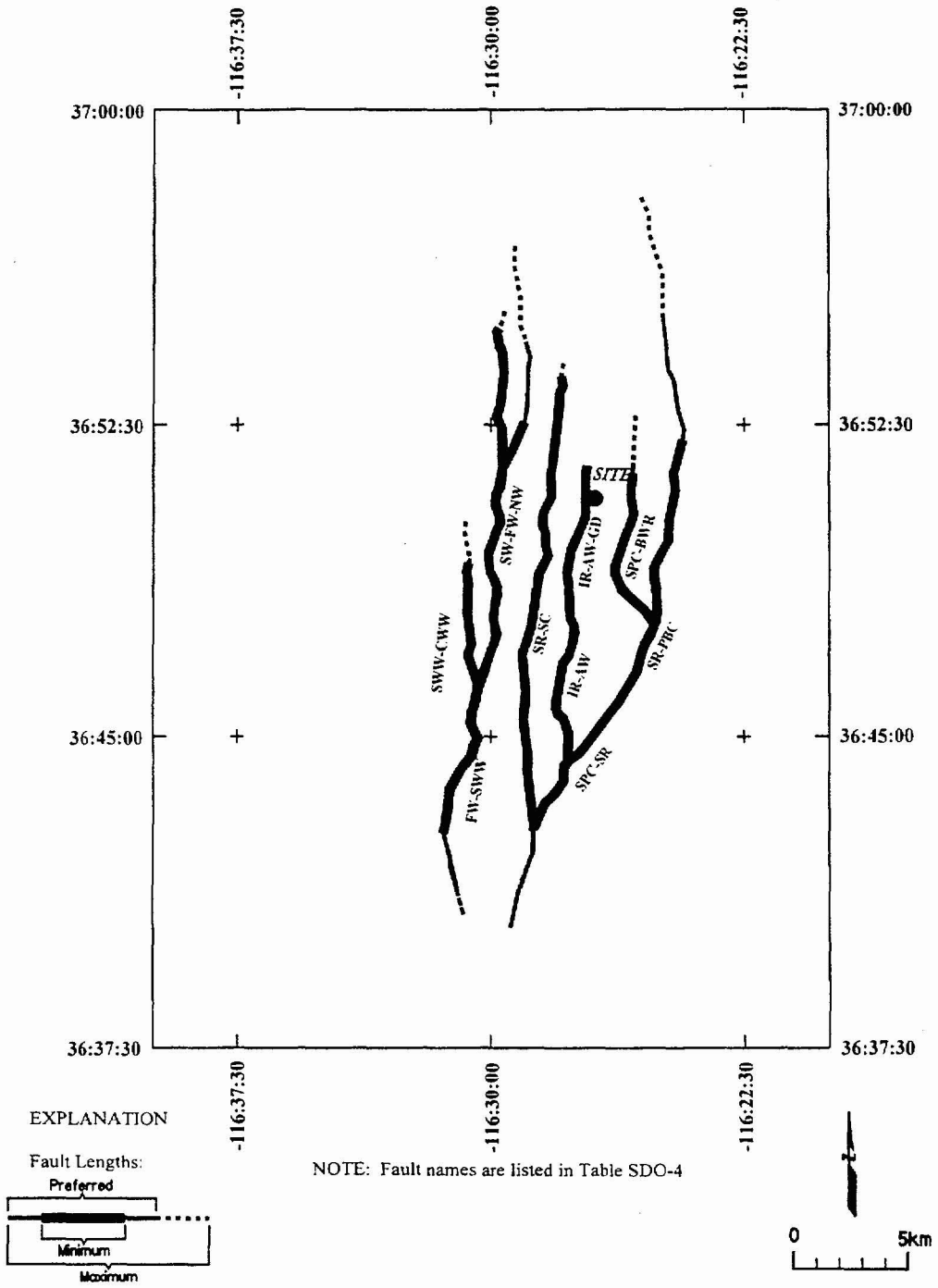


Figure SDO-7b Map showing local fault sources included in the linked seismic source model

h:\prj\yucca_mt\dgn\1097\plate_16_lcl_linked.dgn 07-NOV-1997 10:29

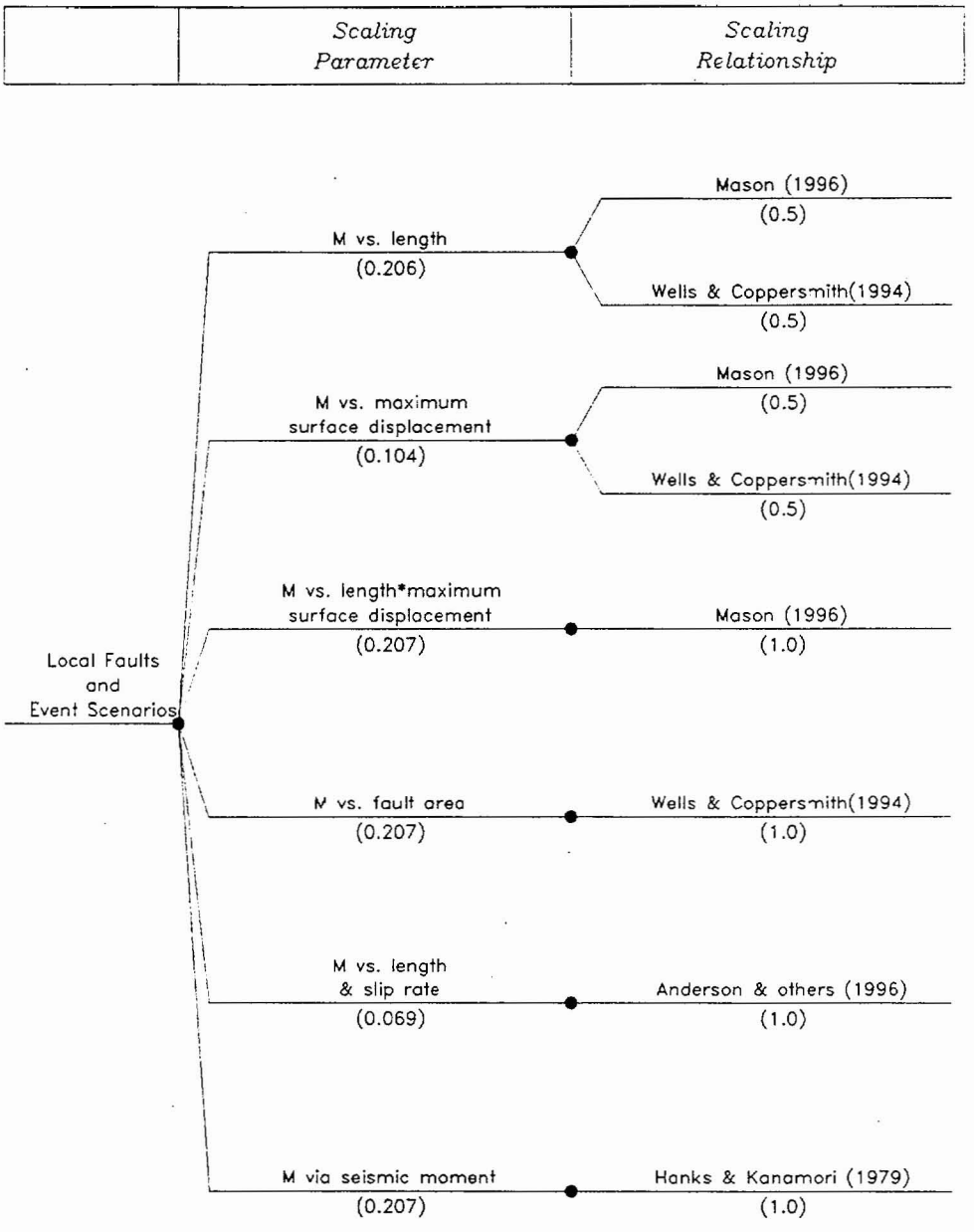


Figure SDO-8 Scaling parameters and relationships used to estimate maximum magnitudes for local faults

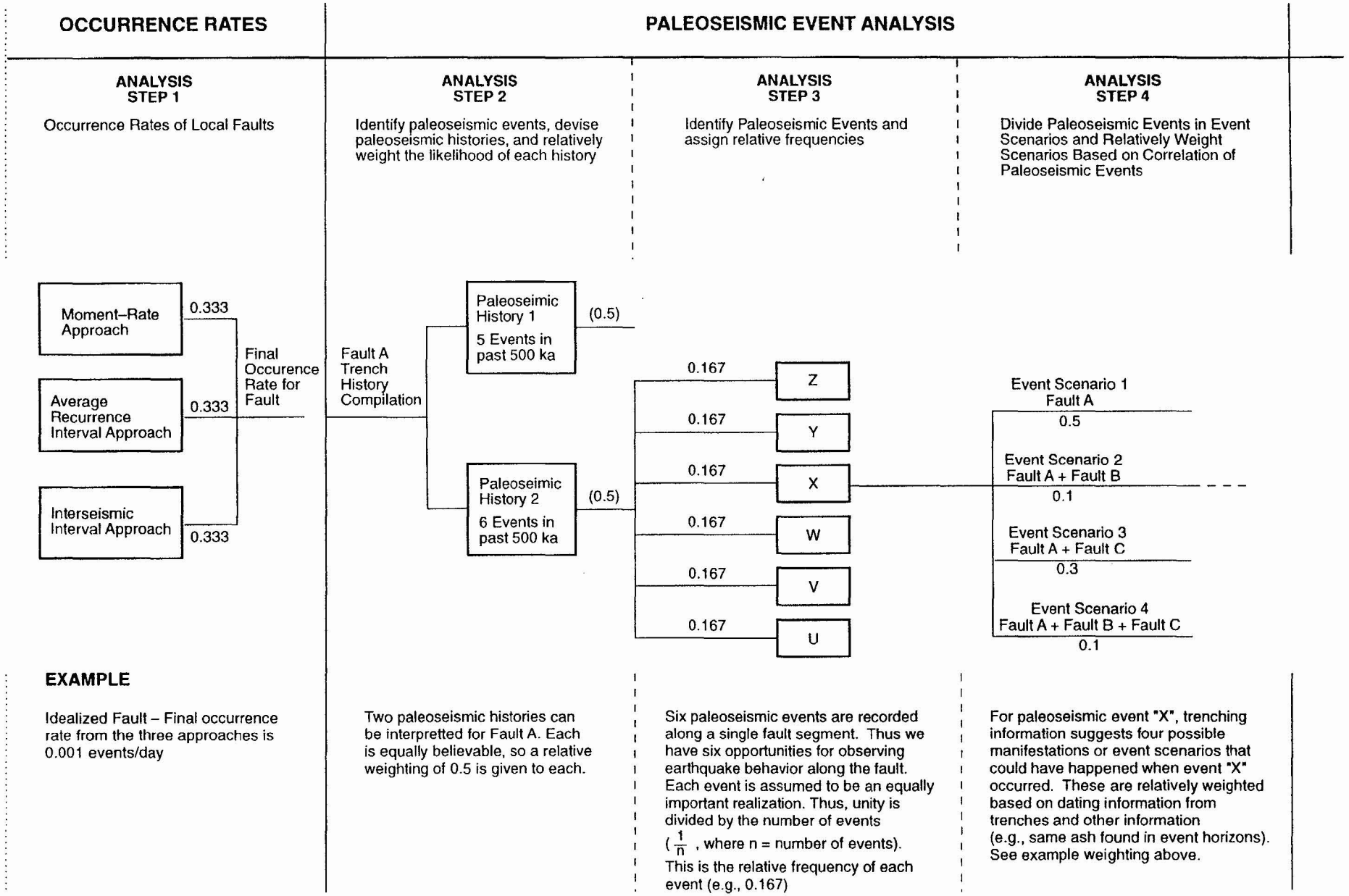


Figure SDO-9 Example calculation of occurrence rates for local faults

## EVENT SCENARIO OCCURRENCE RATES

**ANALYSIS STEP 5**

Calculate Occurrence Rate of Event Scenarios Relative to Individual Paleoseismic Events

**ANALYSIS STEP 6**

Add Up Occurrence Rates for Each Event Scenario from All Paloseismic Events from a Fault that Includes It

**ANALYSIS STEP 7**

Combining Occurrence Rates from Linked and Distributed Event Scenarios

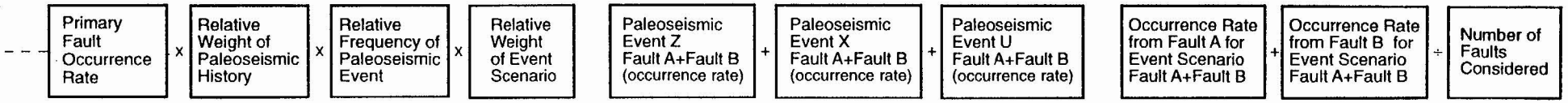


Event X

0.001 x 0.5 x 0.167 x 0.1 ⇒ 8.35E–6

3.34E–5 + 8.35E–6 + 1.67E–5 ⇒ 5.85E–5

5.85E–5 + 7.32E–6 = 6.58E–5 ÷ 2 ⇒ 3.29E–5

Figure SDO-9 Example calculation of occurrence rates for local faults (continued)

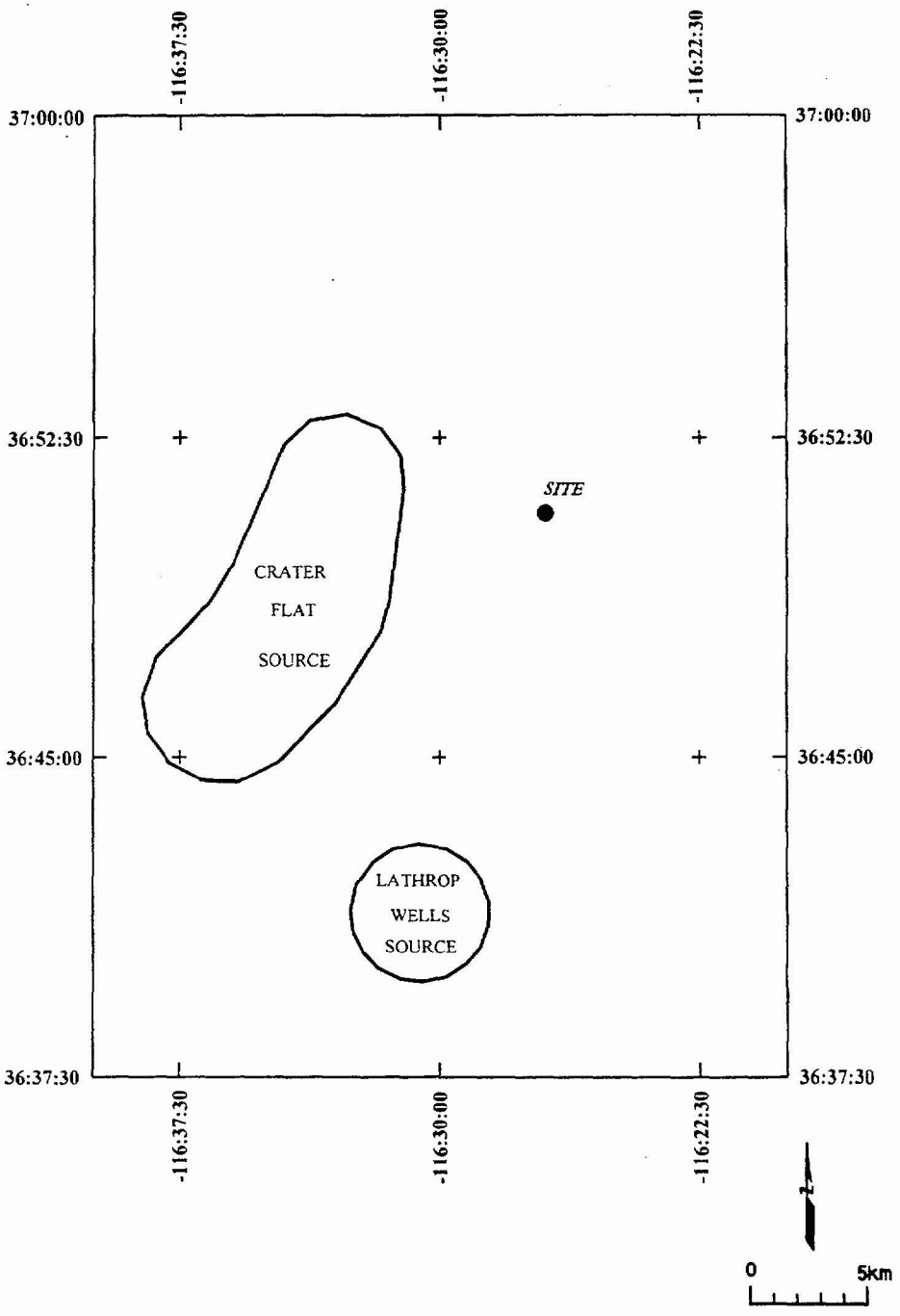


Figure SDO-10 Map showing volcanic zones included in the seismic source model

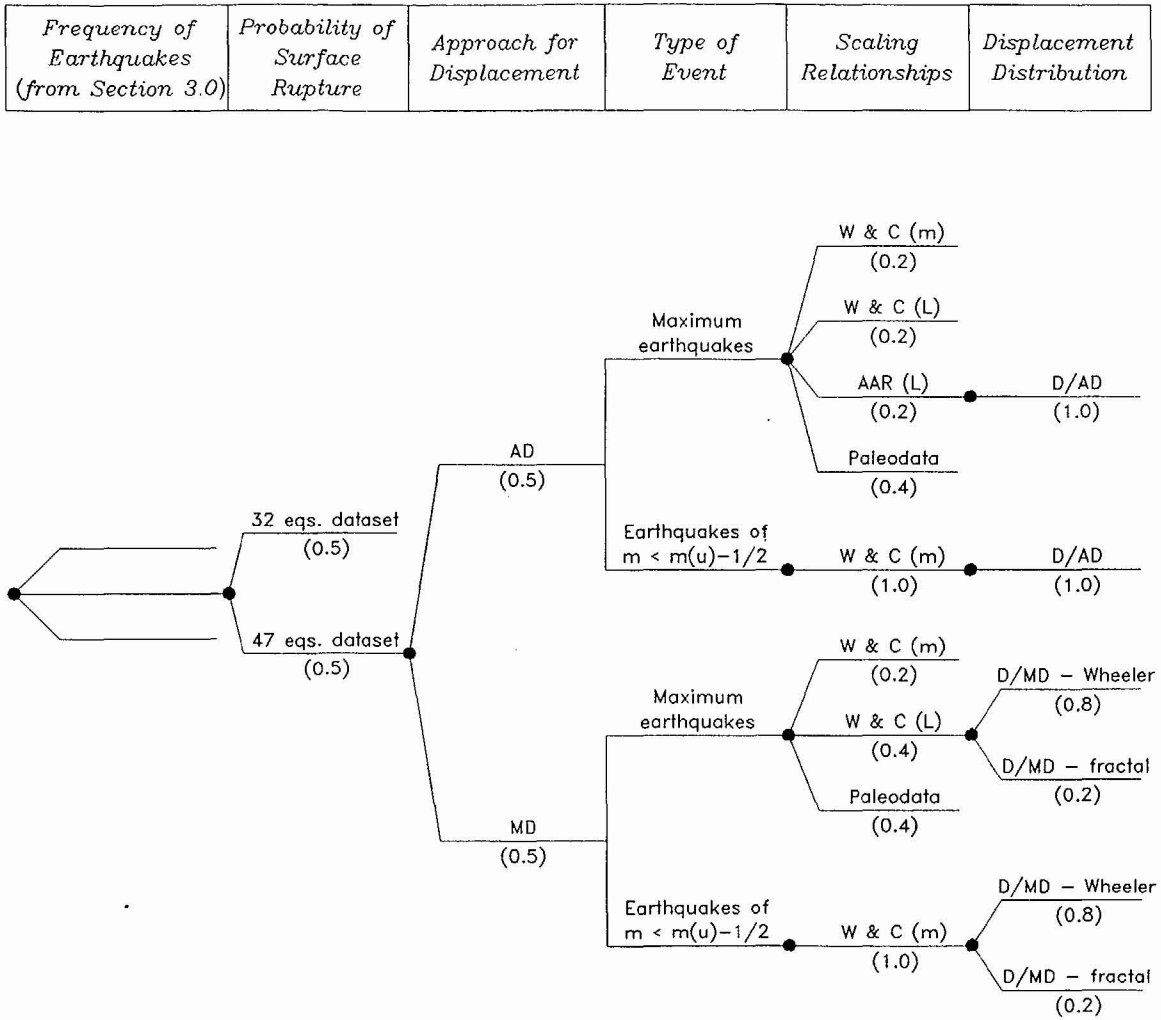


Figure SDO-11 Logic tree used to characterize principal faulting displacement hazard.